Using the Porosity Exponent (*m*) and Pore-Scale Resistivity Modelling to Understand Pore Fabric Types in Coquinas (Barremian-Aptian) of the Morro do Chaves Formation, NE Brazil.

Patrick William Michael Corbett[1,2], Haitao Wang[2], Raphael Nóbrega Câmara[1,3], Ana Carolina Tavares[1], Leonardo Fonseca Borghi de Almeida[1], Fabio Perosi[1], Alessandra Machado[1], Zeyun Jiang[2], Jingsheng Ma[2], Rodrigo Bagueira[4]

[1] Universidade Federal do Rio de Janeiro, Laboratorio de Geologia Sedimentar, Departmento de Geologia, Av. Athos da Silveira Ramos, 274, CEP 21. 941-916, Rio de Janeiro, RJ., Brazil

[2] Heriot-Watt University, Institute of Petroleum Engineering, Edinburgh, EH14 4AS, UK

[3] Now Shell Brasil Petroleo Ltda., Av. Das Americas, Barra do Tijuca, 22640-102, RJ, Brazil

[4] Universidade Federal Fluminese, Instituto de Quimica – Outerio de Sao Batista, CEP 24020-150. Niteroi, RJ, Brazil

Keywords: Coquinas, Carbonates, Petrophysics, Cementation Exponent, Porosity Exponent, *m* exponent, Morro do Chaves Formation, Pore-scale resistivity modelling

Corresponding Author: p.w.m.corbett@hw.ac.uk

Abstract

The recent major discoveries of petroleum in Pre-Salt carbonate reservoirs, of mainly lacustrine origin, offshore Brazil has increased interest in studying these complex non-marine reservoirs, which present many production-development challenges, largely due to their heterogeneous nature. Some of the reservoir carbonate rock-types present in Brazil are limestones composed predominantly of bivalve shells, which are known as 'coquinas'.

The coquinas show a variety of pore types, pore sizes, pore shapes and pore connectivity which define their porosity and strongly influence the permeability and resulting electrical resistivity but this aspect of these relationships in these carbonates has been relatively poorly characterised (particularly in a quantitative manner) in the literature. The petrophysical characterisation of the coquinas of the Morro de Chaves Formation (Barremian-Aptian), exposed in a quarry in NE Brazil, was carried out using the outcrop-selected samples, plugs and petrographic thin-sections to investigate these aspects. Porosity, permeability, grain density and porosity exponent (*m*) measurements were carried out on the plugs. X-ray microtomography was performed to identify key characteristics of the pore system and for the basis of 3-D modelling.

Significant variation in *m* was observed across the plug data set, which is not unexpected in carbonates, but it suggested that a range of fabrics and pore topology were present in these rocks, which are described only as calcirudites. Modelling of the resistivity using 3D pore scale models was used to understand the role of disconnected macro-pores and dissolution seams in controlling the more extreme variation in petrophysical properties observed in the coquinas. This understanding of the controls on resistivity pathways in this outcrop coquina will help in understanding the pore types in the subsurface and the estimation of saturations in these complex rocks where they are found to be oil-bearing.

Introduction

Approximately 50% of the known petroleum reserves in the world are contained in carbonate reservoirs (Ramakrishman *et al*., 2001; Kinoshita, 2007), and carbonates are responsible for some 60% of the world's oil production and 40% of the gas production (Akbar *et al*., 2008; Schlumberger, 2014). It is important to note that most of this production is from carbonates that are marine in origin.

Non-marine, lacustrine carbonate reservoirs have been studied in Brazil in the past, mostly in relation to the coquinas, that form oil reservoirs in offshore fields such as Pampo, Badejo, Linguado and Trilha in the Campos Basin. These reservoirs, known since the 1970's, are important oil reservoirs in the Campos basin (Carvalho *et al.*, 2000) and have been described by Carvalho *et al.* (2000) in terms of their sedimentology, Castro (2006) in terms of their stratigraphy and Baumgarten *et al*. (1988), Horschutz & Scuta (1992) and Horschutz *et al*. (1992), in terms of petrophysical properties. Carvalho *et al.* (2000) highlight that the main lacustrine facies association consists predominantly of bivalves with subordinate ostracods and gastropods locally inter-fingering with siliciclastic facies. In this study, we haven't encountered significant ostracods or gastropods and see some effects of siliciclastic influence. The coquina facies were deposited at the lake margin, with occasional lake level fluctuations giving rise to sub-aerial exposure (Carvalho *et al.*, 2000) which will influence diagenesis and is the subject of related work (Tavares, 2014; Tavares *et al.*, 2015).

Coquinas are defined as concentrations of shells or shelly fragments deposited from the actions of some agent of transport (Schäfer, 1972). The coquinas of the Morro do Chaves Formation are formed by non-marine bivalves and ostracods, with varying terrigenous content and they can sometimes show cross-bedding. The bivalves are thought to have lived in shallow oxygenated water, with their shells being re-transported, and deposited as wash-over fans and beaches that can show a strong storm influence and evidence for long-shore drift on low angle ramps (Thompson *et al.*, 2015). Thompson et al. (2015) highlight the evidence for lacustrine origin of the coquinas but state that to “fully appreciate the hydrodynamic concentration processes, the sorting, orientation and preservation (level of fragmentation and abrasion) of the bioclasts must also be considered”. The comprehensive characterisation of coquinas by petrophysical parameters is relatively poorly discussed in the literature and this paper attempts to shed some light on critical aspects of pore type.

With the recent discoveries of giant petroleum fields in non-marine carbonates (significant coquinas in intervals up to 272m have been reported in Franco Field by ANP (2014) in the Pre-Salt interval of the Santos Basin, these reservoirs have received a revived an increasing interest to understand their sedimentological (Thompson *et al.*, 2015) and petrophysical characteristics. Material from the outcrops of Morro do Chaves Formation in the Sergipe-Alagoas Basin (NE Brazil) has also been used to build a detailed shoreline accretionary beach model using Shark Bay as a modern day analogue (Corbett *et al.,* 2016) following the GPR imaging of a coquina supratidal beach ridge system there by (Jahnert *et al.*, 2012). In such a setting relatively unbroken bivalve shells, sometimes articulated, are intercalated with more abraded broken shells (possibly resulting from storm processes). Additional (local) input of possibly windblown sand or sand from fluvial sources might also be expected.

Rocks that are found in the Morro do Chaves broadly fall into the class of bioclastic calcarenite beach and bar facies (Carvalho *et al.*, 2000), however, detailed facies analysis is not the objective of this study which is focussed on the present day pore structure from a few carefully selected pore types. It’s interesting to note thatinCarvalho *et al.*(2000) shells are shown fully preserved and dominant in the images (partly because of the oil staining). In this study we observe many shells as simple molds, as a result of their dissolution during diagenesis.

The Morro do Chaves Formation outcrops are considered to be analogues for similar facies encountered offshore in the Campos, Santos & Espírito Santo Basins in Brazil and also in West Africa (Congo Basin), where coquinas are present at the same age (late Barremian early Aptian- Jiquiá age (Dale and Lopes, 1990, Azambuja & Arenti, 1998, Harries, 2000; Kinoshita, 2007, Corbett *et al*., 2013, Thompson *et al.*, 2015, Corbett *et al*., 2016) and also form hydrocarbon reservoirs.

Materials and methods

The study was based on outcrop description and samples from coquinas of the Morro do Chaves Formation, that are exposed in a cement quarry known as São Sebastião, at the time of this work operated by Companhia de Cimentos de Portugal (Cimpor Brasil), located near the city of São Miguel dos Campos, Alagoas State, NE Brazil (Fig. 1). This quarry has been traditionally used as an analogue for the offshore coquinas (Kinoshita, 2007). The quarry exposes a vertical thickness of approximately 60m over an extent of 1km in a succession dominated by coquinas, interbedded with minor sandstones (arenites) and shales (Fig.2). A detailed petrographic analysis of these samples (Tavares, 2014; Tavares *et al.,* 2015) has been carried out and only those aspects most relevant to the samples described in this modelling study are included here.

Coquina samples were collected from the succession in the form of nine large oriented blocks from which a total of 53 core plugs were extracted. These blocks and plugs were selected with petrophysical experiments in mind. The blocks were chosen to be large enough to accommodate several plugs, to represent a variety of coquina textural types, and to be transportable under the various restrictions posed by a reconnaissance survey. The location of the nine blocks (PET 1 to PET 9) is shown in Fig. 3 on the stratigraphic section.

The plugs were drilled from the blocks in the lab and then cleaned (in toluene and methanol) and dried in a humid oven at $60^{O}C$ for 24 hours. This is slightly different from current acceptable approaches of $80^{O}C$ in a vacuum oven and $105^{O}C$ in a dry oven. Unless the carbonate contains gypsum or solid hydrocarbon like gilsonite or pyrobitumen there's no need for humidity-controlled drying in carbonates (pers. com. David Bowen) so it appears that humidity-controlled drying was not necessary in this case. Plugs were drilled normal and parallel to bedding fabrics in those blocks that were clearly bedded and in two orthogonal directions selected arbitrarily in the more massive samples. In this way the plugs taken represent horizontal and vertical plugs as taken traditionally in well-bore cores. The 53 plugs underwent analysis for measurement of porosity, permeability (the data is displayed on Fig 4 on a basemap for porosity/permeability data which is discussed further below) and grain density. The porosities and permeabilities were compared with two other unpublished datasets from the same quarry and their representivity as petrophysical exemplars for the quarry was confirmed. The porosity exponent (*m*) was measured on 11 selected plugs. One plug or plug offcut was selected from each of the nine blocks for micro-CT analysis. For comparison, a higher resolution micro-CT volume of a sandstone was used for comparison (sample Fb22 from Arns, 2002).

Porosity – Plug samples were measured by helium expansion with AP-608 equipment, based on the decay of an instantaneous pulse with confining pressure of 1000 psi;

Permeability – Plug samples were measured with AP-608 equipment, based on the decay of an instantaneous pulse decay of nitrogen with a confining pressure of 1000 psi (Câmara, 2013). This data was used to calculate the equivalent liquid permeability, slip and turbulence factors (Schlumberger, 2013). Very small differences between air and liquid permeabilities were observed.

Grain Density – The grain density was calculated by gas expansion injection of helium into a chamber containing the plug sample in an AP-608 device

Porosity Exponent (*m*) –The porosity exponent ``*m*``, is also often referred to as the cementation exponent (Schlumberger, 2017) and is described here in some detail as it forms an important part of this study. The term porosity exponent is preferred as "so-called" cementation (Montaron, 2009) may or may not be the controlling factor on *m* (as it might be in sandstones). The porosity exponent is a key uncertainty, especially in carbonates (Amin *et al.,* 1987, Saha *et al.,* 1993; Adisoemarta, 2000; Ara *et al.,* 2001; Ragland, 2002; Budebes, *et al.*, 2011), in the calculation of water saturation using the Archie equation (Archie, 1942) and the reason that new workflows (Ramakrishnan *et al.,* 2001; Ramamoorthy *et al.,* 2010) and resistivity-independent saturation evaluation techniques have been developed (Ramamoorthy et al., 2012). In order to measure *m* the plugs were saturated in brine of 50,000 ppm NaCl and were left for five days at ambient temperature to stabilise the saturation to ensure ionic equilibrium. Once reaching saturation equilibrium the samples were mounted in a core holder for electrical resistivity measurements at 1000psi confining pressure and ambient temperature. A number of resistivity measurements were taken once the readings stabilised, with no variation for one or two hours. With the brine resistivity (R_w), the length and area of the sample, as well as the resistivity of the rock 100% saturated with brine (R_0), the Formation Factor (FF) and the Porosity Exponent (*m*), were calculated. The *m* is determined from the relationship below, as the gradient on a cross plot of porosity against Formation Factor (FF), ratio of resistivity of brine (R_w) to brine-saturated rock resistivity (R_0), where the Archie factor was assumed to be unity (a = 1 or $R_w = R_0$ at porosity of 100%) in the Archie (FF) Equation:

$$FF = R_w/R_0 = a/\phi^m = 1/\phi^m$$

Micro-CT – Computerised X-ray microtomography (μCT-3D), which also makes an important contribution to this study, was acquired at high resolution with the aim of achieving a better characterisation of the pore space through visualisation of the internal structure of the samples in 3D (Krupinski, 2007; Knackstedt *et al.*, 2007; Remeysen & Swennen, 2008; Machado, 2012; Oliveira, 2012). The *Skyscan* 1173 *High Energy* equipment was used to acquire the data, with a microfocus X-Ray tube, tungsten anode, with a focal point less than 5μm and potential of 8W, operated at energies between 40 to 130kV with a current of 0 to 120μA. The detector used in this μCT was a *flat panel* type with matrix of 2240x2240 *pixels*, with pixel size of 50μm and 12bits of dynamic range. By varying the object-detector distance, a pixel size of 19.7μm was achieved. The objects were 140mm diameter and up to 200mm in length (the plug offcuts were nominally 1-inch in diameter of varying length). Images were obtained operating the μCT at 110kV, current 72μA, aluminium filter (1.0mm) and external copper filter (2.5mm), with steps of 0.3º, rotation of 180º. The details of image processing and the comparison of micro-CT derived porosities with laboratory measured porosities is explained in the Appendix.

Petrophysical Summary

A series of 11 core plug samples (1.5in diameter) were selected in a quarry from a data set of 53 plugs (Fig. 4) for measurement of formation factor (Câmara, 2013). These plugs were essentially twin plugs to the 1in plug offcuts used for the micro-CT imaging (the mico-CT required smaller volumes to get higher resolution, but the FF measurement equipment required larger samples). The gradient (*m*) was determined as a straight line through the porosity equal to 100% and $R_o = R_w$. This assumes the Archie Exponent (*a*) is unity in the Archie Equation. In this way an *m* value is measured for each sample as a measure of pore-scale heterogeneity. This is different from procedures that generate large *m* data sets and look for unique relationships (Budebes *et al.*, 2011) and more appropriate for calibration of pore-scale models investigating the origin of pore-scale heterogeneity (Khalili *et al.*, 2012). The *m* values range from dimensionless 1.7-3.0 for a porosity range of 5-20%. High *m* values are associated with high porosities and permeabilities (Figs 5 & 6). The higher *m* values in the higher porosity was an unexpected result as one would expect more porosity to increase the connectivity and decrease the *m* value.

Three samples covering the range observed in these coquinas were then selected for this numerical study – PET 1, PET 4 and PET 6 – giving a range of *m* exponents in this consistent shell debris-dominated coquina. The measurements were validated in a second laboratory and the comparison found to be acceptable for the purposes of this study (Fig. 7 shows a 1:1 line for comparison between labs and the same relative position of each selected sample is clear). The issue associated with use of different labs was not addressed in this study as the differences between samples were considered greater than the variations observed between laboratories.

The micro-CT volumes were partitioned and a pore network extracted. The details of the partitioning between pore and solid for this study are described fully in Wang

(2015). A simple median filter was used. The porosities estimated visually and measured by various techniques, when compared with the micro-CT porosity suggests that microporosity isn't a significant factor in these particular samples (Câmara, 2013; Wang, 2015) so that the large majority of the porosity is resolved at the 20μm pixel size. Some issues were encountered in sample PET 1 that might be explained by additional microporosity that wasn't resolved and this is discussed later.

Rock Type (Petrotype) Considerations

There are various classifications of rock type existing, with a few classification schemes based on porosity and permeability data, several others are based on capillary pressure data (by injection of mercury) and other rock types are defined by textural definitions. Some examples from the literature are the static petrophysical classification models of Jennings & Lucia (2001), Skalinski & Sullivan (2001), Clerke *et al.*, (2008) and Shenawi *et al.*, (2009) with more recent ones take into account two-phase dynamic flow properties (Skalinski and Kenter, 2015). In this work, we follow the simple porosity-permeability petrotyping scheme described above in order to highlight the significant differences between samples used for screening samples for more detailed petrophysical investigations (as in Corbett & Mousa, 2010). Corbett & Potter (2004) defined petrotype "*as an adequate term to define the members of a finite group of petrophysical types defined by a priori global criteria*". Following these authors, the limits of *petrotypes* are defined by a regular progression of flow zone index (FZI) providing a means for comparing petrophysical aspect in a systematic way across Global Hydraulic Element (GHE) classes.

Carbonate reservoirs are often very heterogeneous in relation to variation in porosity and permeability and range across several GHE's. However, occasionally carbonate reservoirs with a single rock-type, such as certain chalk reservoirs (Corbett and Potter, 2004) are identified. The coquinas are typically more heterogeneous than chalks, occurring in several GHE bands, and that is what is shown for the Morro de Chaves (Fig. 4). Coquinas also appear to be less variable than some carbonates (Corbett and Potter, 2004) suggesting that pore differences are rather more subtle and why the results of this study are interesting for both geological and petrophysical considerations. As petrophysical measurement are often expensive and requiring different samples, and numerical studies very time consuming, studies like this have to be somewhat parsimonious with material studied and the petrotyping provides a useful "reduction of variability" that is often seen in carbonates in order to select, and focus on, key representative samples.

Geological and Petrophysical Description

The porosity encountered in the 53 samples from the Morro do Chaves Formation varies from 4.9 to 21.1%, with permeability varying from 0.052 to 742 mD (Câmara, 2013). Grain density varies from 2.68 to 2.73 g/cm^3, which are broadly consistent for carbonates (calcirudite to calcarenite) where there are also minerals rich in iron and siliciclastic material (predominantly quartz sand grains). The coquinas in this data set are composed predominantly of recrystalised bivalve shells (or their unfilled and filled molds), occasionally with small amounts of terrigenous sand as matrix. Three petrotype samples with varying *m* were selected for this resistivity modelling study and detailed descriptions of the samples are as follows:

Sample PET 1

PET 1 is a bioclastic calcirudite of medium grain-size, poorly sorted, subrounded, normally compacted, principally point and longitudinal contacts, colour cream and white in colour (Fig. 8). The rock is composed mostly of bivalves, with moderate terrigenous influence (about 20%) and formed principally from compacted bivalves reduced to a 'sand' fraction grade. The porosity varies from 10.8 to 14.1% (Fig. 9), with the principal types being moldic/intragranular (55%) and secondary intercrystalline (45%), with less than 1% fracture porosity. The median pore size determined by image analysis is 0.4mm, the maximum observed being 3.36mm. The permeability varies from 12.9 to 36.6mD (Fig. 9). The grain density varies from 2.71 to 2.70 g/cm^3. The average porosity exponent is 1.89. PET 1 is limited to GHE 5 (Fig. 9). The micro-CT shows the interconnected distribution of fine porosity in the 'matrix' whilst the shell moulds are filled with cement (Fig. 10).

Sample PET 4

PET 4 is a bioclastic calcirudite, fine to coarse, poorly sorted, subrounded to subangular, densely compacted, with predominant contacts concave to convex, and light grey to whitish grey in colour (Fig. 11). The rock is composed principally of bivalves, with terrigeneous influence (20 to 30%), principally mono- and poly-crystalline quartz, occurring with a minor proportion of plagioclase, K-feldspar (microcline), lithic fragments of volcanic and metamorphic rocks, and locally rutile. The porosity ranges from 4.9 to 6.5% (Fig. 12), with the principal type of pores being "fracture-like", which are related to low amplitude stylolites/dissolution seams along grain boundaries (70%), followed by moldic/intragranular (30%). The average pore length is 4.5mm and the longest apparent pore (more correctly solution seam system of pores) observed is

37.5mm. The permeability varies from 0.061 to 0.21mD (Fig. 12) and the grain density from 2.68 to 2.70 g/cm^3. The porosity exponent varies from 1.7 to 1.9, with an average of 1.8. PET 4 is found to belong to GHE 3 (Fig. 12). PET 4 is characterised by low porosity and permeability. The principal type of porosity is "fracture-like" and as the fractures present more linear features, the *m* is significantly less than 2. The grain density is less than 2.71g/cm^3, influenced by the siliciclastic material which tends to concentrate along solution seams.

The micro-CT from this facies shows features (Fig. 13) associated with the dissolution of the matrix along seams, forming a closely 'fitted' fabric and some clear dissolution features that are natural and can look like fractures. All the porosity is obliterated by late poikilotopic cement and the remnant porosity is related to fractures and dissolution paths, which are evidence of chemical compaction.

Sample PET 6

PET 6 is a bioclastic calcirudite, fine pebble size, moderately sorted, sub-rounded, loosely compacted, predominantly point and longitudinal contacts, colour cream and white in colour (Fig. 14). The rock is principally composed of bivalves, the terrigenous influence is rare and little matrix is observed (around 10 to 15%) formed from compacted bivalves, which have been reduced to sand-grade fraction. The porosity varies from 15.5 to 21.1% (Fig. 15), with biomoldic (80%) and intercrystalline (20%) porosity, with a median pore-size of 1.55mm, and the largest pores 5.2mm, as observed from digital image analysis. The permeability ranges from 57.9 to 742mD (Fig. 15). The grain density varies from 2.70 to 2.73 g/cm^3. The porosity exponent varies from 2.2 to 3.0, with an average of 2.64. PET 6 is located within GHE 6 between FZI 3-6 (Fig. 15).

This coquina “facies”, of which PET 6 is a typical example, contains the best porosity and permeability in the Morro do Chaves. However, as the main type of porosity is moldic, there are also some isolated molds, which cause connectivity problems so the *m* is also the highest observed in this data set. The mold-size is related to the size of the bivalve shells, with this being related to the depositional energy and the texture of the rock, as shown by the trend within GHE 6 (Fig. 16).

The micro-CT images (Fig. 17) show the large pores which are reasonably well connected (Fig. 9) through the matrix porosity but also appear to have a chance to be isolated. Poikilotopic cement (Tavares, 2014) is present and can be micro-fractured in places adding to flow path complexity. Note that all the samples selected here are broadly described as calcirudites but the following sections will demonstrate that this classification is not enough as the pore systems in this lithotype (geological rock type) is very variable and this has a major impact on the petrophysical properties. We have not considered the other important coquina lithotype – calcarenites – in this study.

Resistivity Modelling

The modelling was carried out on pore space representation extracted from the micro-CT volumes for PET 1, PET 4 and PET 6 (Fig. 18). The formation factor was calculated using a renormalisation technique selected after various other techniques were considered (Khalili, *et al.*, 2012; Wang, 2015) due to its ability to estimate the porosity exponent of the large samples based on the porosity exponent of the small representative samples. In these smaller representative samples, the porosity exponent was also calculated by random walk simulation (Toumelin and Torres-Verdín, 2005 and 2008). Cluster multiple labelling for both 2D and 3D images by Hoshen and Kopelman (1976) known as the

Hoshen-Kopelman algorithm (HKA) was used to identify the main pore cluster which comprises 75% of all pores in PET 4 and PET 6 and 35% in PET 1. The simulated porosity exponent is then based on the largest pore cluster which gives an improvement in computing time on the porosity exponent being simulated for the whole pore space with no loss of accuracy. In this way the resistivity simulation ignores isolated pore clusters, useful when comparing with measurements where isolated pores will carry no electrical current.

Initially a study was undertaken to find the appropriate Representative Elementary Volume (REV) was undertaken (Fig. 19, 20 Top) on micro-CT volumes from PET 1, PET 4 and PET 6 and this was found to be from ca. 350 voxels. At this scale the variability between subsamples decays to a minimum, so this is a scale BELOW which one should not select volumes to carry out simulations. Simulation is often computationally expensive so the priority is to reduce the volume of ‘rock’ (actually CT-volume) that is studied computationally. For different mathematical approaches (e.g. renormalisation) the volume size should be above the REV but as small as possible. With different REV’s in different rocks the reader will see various volumes being used, but always at or above 400 voxels. Initially simulations on 400 x 400 x 400 voxel cubes selected for the modelling study were conducted, as this makes the most efficient use of computing time. Each voxel is about 20 μm so this equates to a block length of 8 mm. This compares with the 2.5 to 3mm REV block length found for the ‘heterogeneous carbonate rock” studied by Khalili *et al.* (2012) but is somewhat larger but still well below the core plug scale so core plugs might be considered volumes above the pore-scale REV for coquinas. This length scale is above the maximum pore size observed in both PET 1 (3.36mm) and PET 6 (5.2mm). PET 4 for has extended pores (up to 37.5mm) and the REV probably accounts for the matrix plus solution seam REV. Identifying the REV for the solution seam network as a whole (potentially much larger volume) is an upscaling study beyond the scope of this study.

In the three samples studied there was reasonable to good agreement with the experimental data (Fig. 20, Bottom). The comparison was very good for the more extreme samples (PET 4, PET 6) than the sample (PET 1) from the middle of the range. The latter difference was analysed in some detail (Wang, 2015) and a better match was found when only the largest pore cluster in PET 1 was analysed suggesting that some of the isolated clusters was causing the higher modelled *m*.

Summary of the current flow density distribution taken from the simulations illustrates the complexity of current flow paths taken in these rocks (Fig. 21). It has been noted before (Haro, 2010) that Archie's Law doesn't take into account direction and these rocks also appear to exhibit significant resistivity anisotropy (Fig. 22). The sub-samples – all above REV scale – were used to investigate porosity and porosity exponent heterogeneity, the ratio of standard deviation to the mean, and anisotropy, the ratio of the maximum to the minimum porosity exponent in three directions (Fig. 22). The coquina samples were found to be significantly more complex than similar experiments done in a sandstone sample (see Wang, 2015, for further details). It has been noted before that complex carbonates require careful upscaling of *m* (Khalili *et al.,* 2012) but this aspect hasn't yet been considered in this study.

Discussion

Initially the correlation of increasing porosity exponent with porosity (Fig. 5) and permeability (Fig. 6) appeared counter-intuitive (although this has also seen before in carbonates examined by Khalili *et al.,* 2012), until the role of unconnected large pores became apparent in the micro-CT images. The presence of unconnected large moldic pores (sometimes with dissolution of adjacent cements and grains which defines *sensu stricto* vuggy pores) could result in the high porosity and relatively low connectivity. The electrical current would flow through the connected pores and not the isolated pores. Using numerical definition of the network allows the pores and pore throats to be "illuminated" (Fig. 23) and the spanning cluster can be extracted from the total pore network (Fig 24). This work was used to prepare a summary for pore types expected in coquinas with moldic unconnected (PET 6), moldic connected/intergranular (PET 1) and fracture (PET 4) (Fig. 25) from Câmara (2013). Intercrystalline systems are only locally present in the coquinas in the Morro do Chaves Formation. This petrophyical summary, for coquinas specifically, is consistent with earlier published work in carbonates in general (Watfa & Nurmi, 1987 and Fig. 26 from Aguilera and Aguilera, 2003). Note that the latter studies refer to vuggy porosity, whereas, here in these coquina samples, the large pores appear dominantly moldic. A key consideration is the criteria of less than 10% of the molds being isolated and this threshold might be difficult to judge in thin sections. Perhaps in resistivity modelling (as in this case) the geological process-related terms molds and vugs can be considered synonymous. It has traditionally been appreciated that the degree of touching (or connected) and non-touching (or non-connected) vugs is an important consideration in carbonate reservoir characterisation (Lucia, 2007) and it is apparent that either molds or vugs will have a different degrees of connectivity. Geological definition of vugs implies greater connectivity. It is the degree of connectivity that is perhaps being detected by the varying *m* exponent. The Schlumberger Oilfield Glossary (Schlumberger, 2017) states "*m* has been related to many physical parameters, but above all to the tortuosity of the pore space" so that connectivity and tortuosity are also being investigated and quantified here through the use of the porosity exponent.

It is perhaps interesting to note that this small data set is characterised by a significant variability in porosity exponent from a single coquina formation at one locality (Wang *et al.*, 2015). This change can be explained by distinct differences in pore-pore throat (Fig. 24, Wang, 2015 using a maximal ball technique after Dong, 2007, to define pores and pore throats). The relatively low values in PET 4 are explained by the presence of quartz grain concentrations along discrete concavo-convex dissolution seams (Fig. 27). Whilst this paper talks about connected and non-connected porosity and the types of pore throat connections, it doesn't aim to separate what petrophysicist would more conventionally recognise as either effective or total porosity. Measurement of additional properties such as the saturation exponent (n) and mercury injection capillary pressure would also help further constrain the understanding of pore topology.

There are very few petrophysical data published from the Pre-Salt Carbonates from Brazil so it is difficult to show the exact nature of the comparison between the oft-quoted Morro de Chaves Formation and the Pre-Salt. As we cannot show a direct coquina comparison, we can show a comparison (Fig. 28) with other Pre-Salt carbonate facies core plugs (possibly including some coquinas) from the North Campos Basin (Chitale *et al.*, 2015). Both Pre-Salt carbonate facies show a high degree of scatter. Exploring the variation in porosity exponent might be a good and cost effective way to help understand this scatter. The plot includes porosity-permeability data from Bed 2b (focus of the study in Corbett *et al.*, 2016) and the detailed petrophysical description of further Bed 2b samples can be found in Luna *et al*. (2016). In the later-conducted but closely-related study, which involved detailed petrophysical analysis of a set of core plugs from a short profile in a single coquina bed from the same quarry site (Bed 2b, at approximately depth 6m on Fig. 3), the range of m values from 1.91 – 2.02 lies in the range of the intergranular pores (PET 1 with average m 1.89) and the moldic pores (PET 6, average m 2.64) so this study presented here helps understand the petrophysical variability seen in different coquina samples.

Mercury Injection Capillary Pressure (MICP) data for PET 1 and PET 6 has been included (Fig. 29). PET 4 data wasn't available because of inevitable budgetary restrictions in the project and the consequent focus on acquisition in the better quality reservoir rocks. A micro-porosity (defined by pore throat radius of 0.5microns) was seen in PET 1, and this may explain the differences between higher modelled *m* compared with measured *m* as observed in Fig. 20, as microporosity reduces *m* (Ragland, 2002). Note that all the pore throats in these samples are below 10μm and below resolution of the micro-CT. Experience in related NMR studies in coquinas from the same quarry shows micropores generally to be minor (quantified as less than 4% of the total NMR porosity, Luna *et al.,* 2016). Micro-porosity as defined by pore throats (MICP) and pore size (NMR) appear to be inconsistent but this aspect was not investigated further in this study.

Conclusions

A resistivity measurement and modelling study in the coquinas of the Morro de Chaves Formation has been carried out on three petrotype calcirudite samples which are characterised as follows:

- PET 1 is characterized by low values of *m*, around 1.89, and shows intermediate porosity and permeability with well-connected matrix porosity and shell moulds that are dominantly infilled. Best match between measured and modelled *m* was achieved when only the dominant cluster was modelled.

- PET 4 shows the lowest values of porosity and permeability, but also the lowest tortuosity, due to solution-seam related, ‘fracture-like’, porosity in micro-stylolites and (dis-)solution seams/channels. It is characterized by an average *m* of 1.8.
- PET 6 showed characteristics of a high-energy depositional environment, which were reflected in high porosity, high permeability and high *m* (3.0) due to the presence of non-connected moldic porosity (or in some cases vugs).

In this study, an appropriate length of REV for coquinas is 600 voxels (12 mm block length) well above the minimum REV of 350 voxels and this could be used as the starting point for any further numerical simulations in these rocks. This is significantly smaller than core plug volumes but well above the maximum pore size (5.2mm in PET 6). Using supra-REV-sized sub-samples we have considered heterogeneity and anisotropy for carbonate porosity exponent (*m*) and showed that there is a strong directional control. The porosity exponent (*m*) is determined as the mutual effect of pore size, length and pore types.

These rocks are all described as calcirudites. Pore types for these three coquina petrotypes are dominated by:

- Intergranular pore (IG) in PET 1
- Fracture-like pore (FT) and reduced porosity exponent in PET 4. Rather than fractures PET4 has concavo-convex pore network of dissolution seams.
- Moldic or vuggy pore (VG) and increased porosity exponent in PET 6

Whilst only three samples were subjected to a very detailed modelling study – such data in Brazil are difficult to come by - it was considered pragmatic to use the GHE approach to select different samples for measurement of formation factor and from those we selected the extreme and a sample from the centre of the variation in *m* observed. We believed this Petrotyping screening method revealed interesting and significant results. The petrophysical properties in the Morro do Chaves Formation appear to be controlled by a combination of depositional fabric and diagenetic alteration like many other carbonates. With the petrophysical results to hand, drawing attention to significant differences whilst reviewing the petrographic images, it has been possible to quantify and describe the significant differences in pore types and their effect on the porosity exponent. The depositional energy and the texture have a large influence and control on the porosity of PET 6. As the principal porosity type is moldic, which occasionally develop into vugs by the dissolution of interparticle cement (forming connected molds), these isolated large pores will significantly affect the porosity exponent. Diagenesis is the principal factor which seems to control porosity in PET 4 through the development of solution seams which concentrates the siliciclastic grains which have small intergranular pores. The large variation is seen in the macro- and micro-scale and results from various dissolution and precipitation events. Further work is needed to refine the correlation between depositional facies, diagenetic facies and petrophysical facies (Câmara, 2013; Tavares, 2014; Tavares *et al.*, 2015) in these complex rocks and this work is still ongoing in the SACL project, guided by the recognition of key pore types described here. This work will help identify further samples in the laboratory to source large numbers of sample material for various reservoir engineering core flood studies.

We note that varying *m* in coquinas will also result in uncertainty in water saturation (Sw) requiring the percentage of IG, FT, VG pore types to be estimated during geological core logging (where core is available) to help constrain petrophysical facies in cored wells and to map the link to depositional/diagenetic textures. This will impact the estimation of oil-in-place in any coquina reservoir unit and should be considered in any coquina reservoir study.

Acknowledgements

This work was carried out during as part of the ongoing SACL (Sergipe-Alagoas Carbonate Laboratory) Project, registered as "Análise geológica sedimentar de sucessões carbonáticas cretácias em uma bacia sedimentar brasileira" (Fundação Coppetec proj. IGEO 15.981; UFRJ/BG Brasil/ANP) and funded by BG Brasil under the ANP R&D levy programme known as "Compromisso de Investimentos com Pesquisa e Desenvolvimento". Patrick Corbett was funded by BG Group for a two year assignment in UFRJ in connection with the SACL project. The support of Cimpor Quarries was fundamental and Christianne Acioli and Aline Goes are thanked for their help and support. Schlumberger Geoengineering and Research Centre in Rio (Esperanza Noriega & Eudes Muniz) are acknowledged for their support with the plugging and carrying out the petrophysical measurements. Frances Abbots (BG Group Technology, now Shell) has been a valued reviewer of the SACL project throughout and has contributed to its success in many ways. Christoph Arns (Australian National University) is thanks for making the CT scans of sample Fb22 available.

Finally, Bob Ransom, who taught the primary author petrophysics in the 1980's, is thanked for his timely reminder in the pages of Petrophysics (August 2014) that we should in his opinion refer to *m* as the porosity exponent and not the cementation exponent as in coquinas the exponent reflects complex 'non-cementation' (i.e., dissolution) and resulting connectivity issues. As a parameter that is relatively simple to measure non-destructively, it is also very valuable to assist the geologists in understanding the nature of complex carbonate pore systems found in carbonates such as coquinas!

Appendix

Resolving micro-CT porosity and the comparison with porosimeter porosity

With any micro-CT study there are always questions about the thresholding. The resolution of porosity is discussed in detail (see Appendix B, Wang, 2015 from which the following sections are taken). In this study, a long flat trough between the pore peak and the matrix peak was found on the grey scale images (Fig. A1) making it difficult to manually select the appropriate threshold value for pores and solid. A manual selection was compared with the "Auto" selection option in ImageJ (refer to http://iamgej.nih.gov/ij/), a comparison made, and the appropriate threshold selected.

The median was applied using the Process – Filters – Median option in Image j. The radius of the 2D region where the average of the grey scale data is used to replace the grey scale at the point centred in the region. This radius was selected manually and results reviewed and an appropriate filter selected (Fig. A2 and A3).

A comparison of pore radius and pore throat radius extracted from the micro-CT volumes is shown in Fig. A4 alongside a sandstone sample for reference. The resolution of the Fb22 sample at 5.68μm is lower than the PET 1, 4 and 6 samples at 19.27 μm, but it is clear that the sandstone sample has smaller pore and pore throat size. The plots suggest that all the pores in the coquina samples are adequately resolved but that some pore throats, particularly for PET 4, are undersampled. In this sample the addition of a small amount of sub-micro-CT- resolution microporosity will only increase the pore connectivity and tend to further reduce the *m* exponent in the simulations.

Finally, as a check on the micro-CT porosity extracted, a comparison was made with helium-expansion porosimeter measured on adjacent plugs to the micro-CT volumes (Fig. A6) and these are considered reasonably comparable given the nature of carbonate pore systems.

References

Adisoemarta, P.S., Anderson, G.A., Frailey, S.M., and Asquith, G.B., 2000, Historical use of *m* and *a* in well log interpretation: is conventional wisdom backwards? Society of Petroleum Engineers, SPE 59532, Midland, 1-07.

Aguilera, R. and Aguilera, M.S., 2003, Improved models for petrophysical analysis of dual porosity reservoirs, Petrophysics, Vol. 44, No. 1, 21-35.

Akbar, M., Steckhan, J., Tamimi, M., Zhang, T., and Saner, S., 2008, Estimating Cementation Factor (*m*) for Carbonates Using Borehole Images and Logs. In: Society of Petroleum Engineers, Abu Dhabi International Petroleum Exhibition and Conference, Abu Dhabi, United Arab Emirates, 1-10.

Amin, A.T., Watfa, M., and Awad, M.A., 1987, Accurate estimation of water saturation in complex carbonate reservoirs. SPE 15714. Society of Petroleum Engineers Middle East Oil Show, Manama, Bahrain.

ANP, 2017, http://geofisicabrasil.com/noticias/55-governo21/870-anp-segundo-poco-tao-grande-quanto-primeiro.html accessed 25/5/2017

Ara, T.S., Talabani, S., Vaziri, H.H., and Islam, M.R., 2001, Depth investigation of the validity of the Archie equation in carbonate rocks. SPE 67204, Society of Petroleum Engineers, Oklahoma, United States, 1-10.

Archie, G.E., 1942, The electrical resistivity log as an aid in determining some reservoir characteristics. Transactions of the American Institute of Mining, Metallurgical and Petroleum Engineers, v.146, 54-62.

Arns, C.H., *The influence of morphology on physical properties of reservoir rocks*. 2002, PhD Thesis, The University of New South Wales.Sydney, 277p.

Azambuja, N.C., and Arienti, L.M., 1998, Guidebook to the Rift-Drift Sergipe-Alagoas, Passive Margin Basin, Brazil. The 1998 American Association of Petroleum Geologists International Conference and Exhibition.113p.

Baumgarten, C.S., Dultra, A.J.C., Scuta, M.S., Figueiredo, M.V.L.,and Sequeira, M.F.P.B., 1988, Coquinas da Formação Lagoa Feia, Bacia de Campos: evolução da Geologia de Desenvolvimento. Boletim de Geociências da Petrobrás, Rio de Janeiro, v.2, n.1, 27-36.

Budebes, S., Saif, O., Al-Farisi, O., Hamdy, T., Al-Marzouqi, M., and Yammahi, F., 2011, Carbonate Archie exponents correction model and variable determination. SPE, 148377, Society of Petroleum Engineers. Abu Dhabi, United Arab Emirates, 1-06.

Câmara, R.N., 2013, Caracterização petrofísica de coquinas da formação morro do chaves (barremiano/aptiano), intervalo pré-sal da bacia de Sergipe-Alagoas. Programa de Pós-graduação em Geologia, Instituto de Geociências, Universidade Federal do Rio de Janeiro, Dissertação de Mestrado, 112p.

Carvalho, M.D. Praca, U.M., and Telles, A.C.S., 2000, Bioclastic Carbonate Lacustrine Facies Models in the Campos Basin (Lower Cretaceous), Brazil. In: Gierlowski–Kordesch, E.H., and Kelts, K.R. Lake Basins Through Space and Time: American Association of Petroleum Geologist Studies in Geology 46, 245–256

Castro, J. C., 2006, Evolução dos conhecimentos sobre as coquinas-reservatórios da Fomação Lagoa Feia no *trend* Badej-Pampo-Linguado, Bacia de Campo. **Geociências** (UNESP), São Paulo, v. 25, n. 2, 175-186.

Chitale, V., Alabi, G., Garmin, Lepley, S., Piccoli, P., 2015, Reservoir Characterization Challenges due to Multiscale Reservoir Heterogeneity in the Pre-Salt Carbonate Sag Formation, North Campos Basin, Brazil, Petrophysics, 56(6), 552-576.

Clerke, E.A., Mueller, H.W.III., Phillips, E.C., Eyvazzadeh, R.Y, Jones, D.H., Ramamoorthy, R.,and Srivastava, A., 2008, Application of Thormeer Hyperbolas to decode the pore systems, facies and reservoir properties of the Upper Jurassic Arab D Limestone, Ghawar Field Saudi Arabia: A “Rosetta Stone” approach, GeoArabia, 113-160.

Corbett, P.W.M., and Potter, D., 2004, Petrotyping: A basemap and atlas for navigating through permeability and porosity data for reservoir comparison and permeability prediction. SCA Annual Conference, Abu Dhabi, 01-12.

Corbett, P.W.M., and Mousa, N., 2010, Petrotype-based sampling to improved understanding of the variation of Saturation Exponent, Nubian Sandstone Formation, Sirt Basin, Libya, Petrophysics, 264-270.

Corbett, P.W.M., Câmara, R., Monteiro, R., Tavares, A. C. G., Teixeira, B., and Borghi, L., 2013, Framework for modeling of wireline log response from carbonate outcrops. Sociedade Brasileira de Geofísica, Thirteenth International Congress of the Brazilian Geophysical Society, Rio de Janeiro, 01-03.

Corbett, P.W.M., Estrella, R., Shoier, A., Morales, A., Borghi, L. and Tavares, A. C., 2016, Integration of Cretaceous Morro do Chaves rock properties (NE Brazil) with the Holocene Hamelin Coquina architecture (Shark Bay, Western Australia) to model effective permeability, *Petroleum Geoscience*, v22, 105 – 122

Dale, C.T., and Lopes, J.R., 1990, Takula Oil Field and the greater Takula Area, Cabina, Angola.Offshore Technology Conference, Houston, 635-644.

Dong, H., 2007, Micro-CT imaging and pore network extraction, Unpubl PhD Thesis Imperial College, London, 217p.

Haro, C.F., 2010, The equations Archie forgot: anisotropy of the rocks. Annual Technical Conference and Exhibition. Society of Petroleum Engineers, New Orleans, United States, 823-836.

Harris, N.B., 2000, Toca Carbonate, Congo Basin: response to an evolving rift lake. In: Mello, M.R.; Katz, B.J. (eds.). Petroleum Systems of South Atlantic Margins: American Association of Petroleum Geologists, Memoir 73, v.73, 341–360.

Horschutz, P. M. C., andScuta, M.S., 1992, Fácies-perfis e mapeamento de qualidade do reservatório de coquinas da Formação Lagoa Feia do Campo de Pampo. Boletim de Geociências da Petrobrás, Rio de Janeiro, v.6, n.1/2, 45-58.

Horschutz, P.M.C., Freitas, L.C.S., Stank, C.V., Barroso, A.S.,and Cruz, W.M., 1992, The Linguado, Carapeba, Vermelho and Marimbá Giant Fields, Campos Basin, Offshore Brazil. Halbouty, M.T. (eds.) Giant oil and gas fields of the decade, 1978-1988. Tulsa: American Association of Petroleum Geologists, Memoir 54, v.54, 137-153.

Hoshen, J., and Kopelman, R., 1976, Percolation and cluster distribution, Phys. Rev. B 1(14) 3438-3445

Jennings, J.W Jr. and Lucia, F.J., 2001, Predicting permeability from well logs in carbonates with a link to geology for interwell permeability mapping, Society of Petroleum Engineers, Louisiana.

Jahnert, R., de Paula, O., Collins, L., Strobach, E., & Pevzner, R., 2012, Evolution of a coquina barrier in Shark Bay, Australia by GPR imaging; Architecture of a Holocene Reservoir Analogue, Sed. Geol. 281, 59-74.

Khalili, A.D., Yanici, S., Cinar, Y., and Arns, C.H., 2012, Formation Factor for heterogeneous carbonate rocks using multi-scale X-ray-CT images. Kuwait International Petroleum Conference and Exhibition, Society of Petroleum Engineers, Kuwait City, Kuwait, 01-13.

Knackstedt, M.A., Arns C.H., Sheppard, A.P., Senden, T.J., Sok, R.M., 2007, Archie's exponents in complex lithologies derived from 3d digital core analysis. Society of Petrophysicists and Well Log Analysts 48th, Annual Logging Symposium, Texas, United States, 01-16.

Kinoshita, E.M., 2007, Modelagem sísmica-geométrica de fácies dos carbonatos lacustres do Mb. Morro do Chaves, Bacia de Sergipe-Alagoas. Dissertação (Mestrado em Geologia), Instituto de Geologia, Universidade Federal do Paraná, Curitiba, 97p.

Krupinski, E.A., Williams, M.B., Andrieole, K., Strauss, K.J., Applegate, K., Whyatt, M., Bjork, S., and Seibert, A., 2007, Digital radiography image quality: image processing and display. Journal of the American College of Radiology, 4, (6), 389-400.

Lucia, F. J., 2007, Carbonate Reservoir Characterisation: An Integrated Approach, Springer, 354p , **ISBN-13:** 978-3540727408.

Luna, J. L. de, Perosi, Ribeiro, M. G. dos S., F. A., Souza, A., Boyd, A., Borghi de Almeida, L. F., and Corbett, P.W.M., 2016, Petrophysical Rock Typing of coquinas from the Morro do Chaves Formation, Sergipe-Alagoas Basin (North-east Brazil), Revista Brasileira de Geophysica, 34(4).

Machado, A. C., 2012, Estudo de parâmetros microestruturais de rochas-reservatório para diferentes resoluções utilizando microtomografia computadorizada 3D. Dissertação (Mestrado em Engenharia Nuclear) - Programa de Pós-graduação em Engenharia Nuclear, COPPE, da Universidade Federal do Rio de Janeiro, Rio de Janeiro, 57p.

Montaron, B., 2009, Connectivity Theory – A new approach to modelling non-Archie rocks, Petrophysics, 50(2), 102-115.

Mitchell, L., 2014, Dissolution features within a core plug taken from the Morro do Chaves Formation, Sergipe-Alagoas Basin, Northeast Brazil, Unpubl. MSc Thesis, Heriot-Watt University, 31p.

Oliveira, M.F.S., 2012, Estudo de parâmetros microestruturais de rochas-reservatório para diferentes resoluções utilizando microtomografia computadorizada 3D.Tese (Doutorado em Engenharia Nuclear) - Programa de Pós-graduação em Engenharia Nuclear, COPPE, da Universidade Federal do Rio de Janeiro, Rio de Janeiro.149p.

Ragland, D.A., 2002, Trends in cementation exponents (m) for carbonate pore systems. Society of Petrophysicists and Well Log Analysts, 43(5), 434-446.

Ramakrishnan, T.S., Ramamoorthy, R., Fordham, E., Schwartz, L., Herron, M., Saito, N., and Rabaute, A., 2001, A model-based interpretation methodology for evaluating carbonate reservoirs. The Society of Petroleum Engineers Annual Technical Conference and Exhibition, New Orleans, 01-15.

Ramamoorthy, R., Boyd, B., Neville, T.J., Seleznev, N., Sun, H., Flaum, C., and Ma, J., 2010, A new workflow for petrophysical and textural evaluation of carbonate reservoirs, Petrophysics, 51(1), 17-31.

Ramamoorthy, R., Boyd, A., Ferraris, P, 2012, SPWLA Short Course Notes, Cartagena, June 16.

Remeysen, K., and Swennen, R., 2008, Application of Microfocus computed tomography in carbonate reservoir characterization: Possibilities and limitations. Marine and Petroleum Geology, 25(6), 486-479.

Saha, S., Asquith, G.B., and Drager, L., 1993, A new approach to estimating Sw in carbonate reservoirs, The Log Analyst, 34(3), 20-25.

Schafer, W., 1972, Ecology and Paleoecology of Marine Environments. Chicago: The University of Chicago Press, 568p.

Schlumberger, 2013, Routine Core Analysis and Formation Factor, Confidential Report prepared for Universidade Federal do Rio de Janiero, Sept., 2013.

Schlumberger, 2014, http://www.slb.com/services/technical_challenges/carbonates.aspx , accessed 5/12/2014

Schlumberger, 2017, http://www.glossary.oilfield.slb.com/Terms/p/porosity_exponent.aspx viewed 29/3/2017

Shenawi, S., Al-Mohammadi, H. and Faqehy, M., 2009, Development of generalized porosity-permeability transforms by hydraulic units for carbonate oil reservoirs in Saudi Arabia. Society of Petroleum Engineers 126073, SPE Saudi Arabia Technical Symposium and Exhibition, Saudi Arabia.

Skalinski, M.T. and Kenter, J., 2015, Carbonate petrophysical rock typing: Integrating geological attributes and petrophysical properties while linking with dynamic behavior, in Agar, S., and Geiger, S., Fundamental controls of fluid flow in carbonates, Current workflows to emerging technologies, Geol. Soc. Spec. Publ., 406, 229-239.

Skalinski, M.T. and Sullivan, M.J., 2001, Application of improved method for permeability estimation in complex lithology reservoirs. SPWLA 42nd annual logging symposium, 01-14.

Tavares, A.C., 2014, Fácies diagenéticas em coquinas da Formação Morro do Chaves (Barremiano/Aptiano da Bacia de Sergipe-Alagoas), MSc Thesis, Instituto de Geociências, Universidade Federal do Rio de Janeiro - UFRJ, Rio de Janeiro,196p.

Tavares, A. C., Borghi, L., Corbett, P.W.M., Lopes, J., Câmara, R., 2015, Facies and depositional environments for the coquinas of the Morro do Chaves Formation, Sergipe- Alagoas Basin, defined by taphonomic and compositional criteria, Brazilian Journal of Geology, 45(3), 415-429

Thompson, D.L., Stilwell, J.D., and Hall, M., 2015, Lacustrine carbonate reservoirs from Early Cretaceous rift lakes of Western Gondwana: Pre-Salt coquinas of Brazil and West Africa, Gondwana Research (2015), http://dx.doi.org/10.1016/j.gr.2014.12.005

Toumelin, E. and Torres-Verdín, C., 2005, "Influence of oil saturation and wettability on rock resistivity measurements: a uniform pore-scale approach". Paper PPP in

SPWLA 46th Annual Logging Symposium, New Orleans, Louisiana, USA, 26-29 June. Society of Petrophysicists and Well-Log Analysts, 1-14.

Toumelin, E. and Torres-Verdín, C., 2008, "Object-oriented approach for the pore-scale simulation of DC electrical conductivity of two-phase saturated porous media". Geophysics, 73(2): E67-E79.

Wang, H., 2015, Numerical Simulation of Resistivity and Investigation of Porosity Exponent in Carbonates, Heriot-Watt University, Unpubl. PhD, 285p.

Wang, H., Corbett, P.W.M., and Jiang, Z., 2015, Archie's Porosity Exponent: REV, Heterogeneity and Anisotropy in a Coquina Carbonate, Abstract EAGE Madrid, June 2015

Watfa, M. and Nurmi, R., 1987, Calculation of saturation, secondary porosity and producibility in complex Middle East carbonate reservoirs. The Society of Petrophysics and Well Log Analyst 28th Annual Logging Symposium, London, n.02, 01-24.

Lithology	PET Samples	ϕ (%)	k (mD)	Rho_g (g/cm^3)	*m*	GHE
Calcirudite	5	14.3	160	2.71	2.16	4-7
Calcirudite	3,6,9	17.8	158	2.72	2.64	6
Calcarenite	2,7	16.3	26.7	2.70	2.2	4-5
Calcirudite	1	11.7	18.1	2.70	1.89	5
Calcirudite	4,8	5.6	0.12	2.69	1.8	3

Table 1 –Summary of lithological description for PET samples 1-9, ordered by reservoir quality, with average values for porosity, permeability, grain density, *m*, and GHE designation for related samples. Note: PET 1, 4, 6 are all calcirudites with matrix density close to that of calcite (2.71 gm/cm^3)

Nomenclature

ANP	National Petroleum Agency (Brazil)
CT	Computer Tomography
ϕ	Porosity
Fb	Fontainebleau (as in sandstone sample Fb22)
FF	Formation Factor
FT	Fracture-type pore system
GHE	Global Hydraulic Element
GP	Renormalisation Algorithm (Green - Paterson)
GPR	Ground Penetrating Radar
IG	Intergranular pore system
K	Potassium (as in K Feldspar)
KK	Renormalisation algorithm (Karim-Krabbenhoft)
m	Archie Porosity Exponent (also known as Cementation Exponent)
mD	milledarcy
MICP	Mercury Injection Capillary Pressure
NMR	Nuclear Magnetic Resonance
PET	Petrophysical sample
psi	Pounds per square inch
REV	Representative Elementary Volume
Rho	Density
R_w	Brine resistivity
R_o	Brine saturated rock resistivity (Sw = 1)
S_w	Water Saturation
SACL	Sergipe-Alagoas Carbonate Laboratory
UFRJ	Universidade Federal do Rio de Janeiro
VG	Vugular or Moldic Pore System

Figures

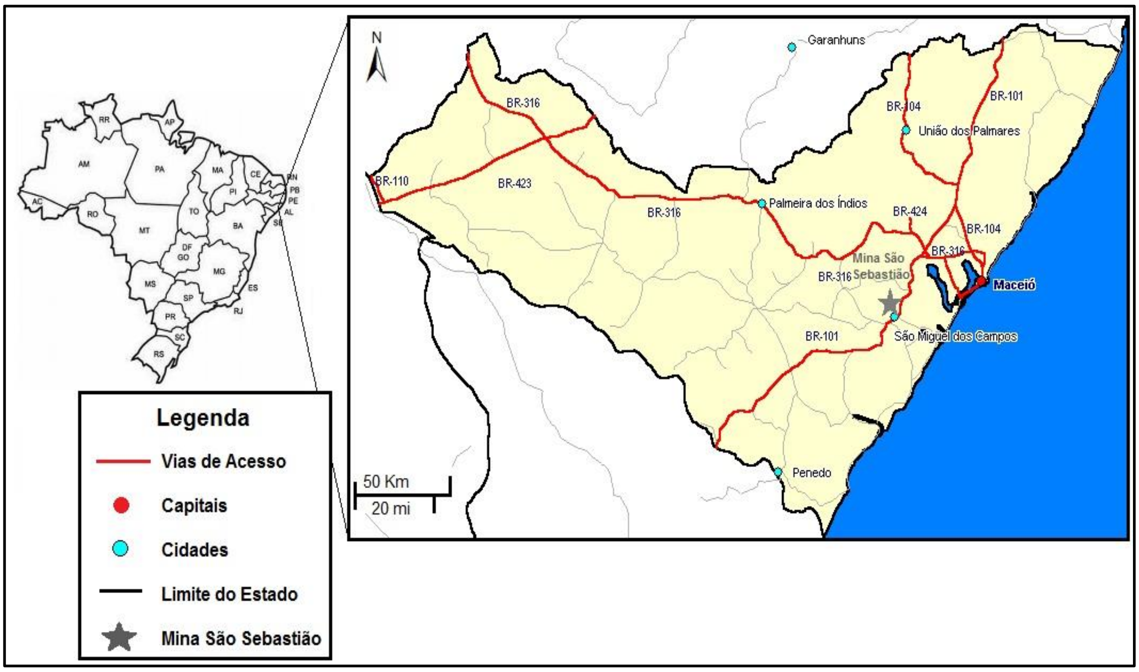

Figure1 –Locality map for the São Sebastião Quarry located near the town of São Miguel dos Campos, Alagoas State, NE Brazil.

Figure2 –Quarry face, Morro do Chaves Formation, on the east side of the São Sebastião Quarry. Outcrop of approximately 60m of meter-scale beds of coquinas (intervals of cream and light grey colour) intercalated with shales (intervals of dark grey and greenish grey).

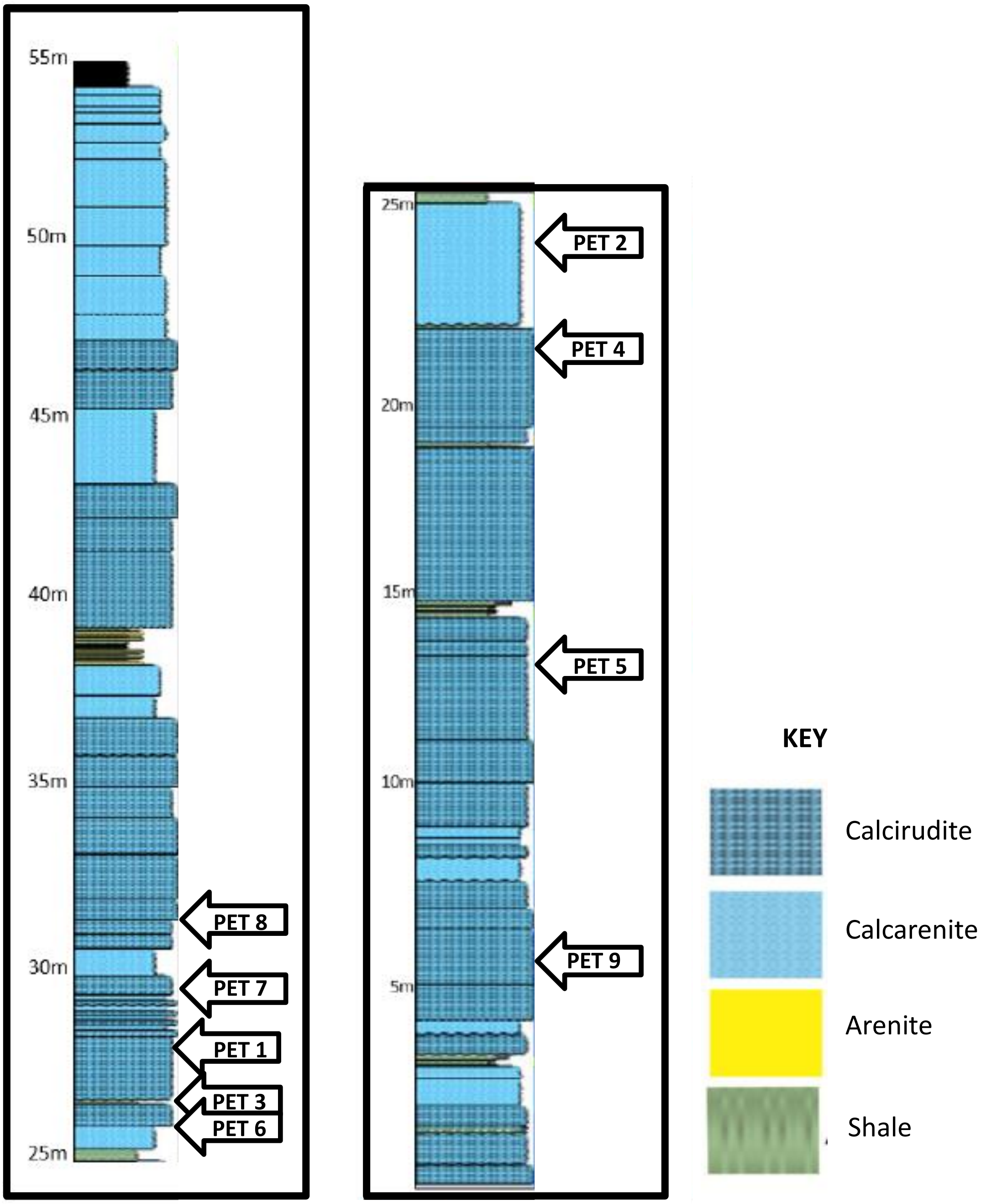

Figure 3–Stratigraphic location of the 9 petrophysical samples (PET 1-9) in the Morro do Chaves Formation, on the east side of the São Sebastião Quarry. The section is taken from Tavares, 2014 where further detailed description can be found. Section mostly composed of calcirudite which is the focus of this study.

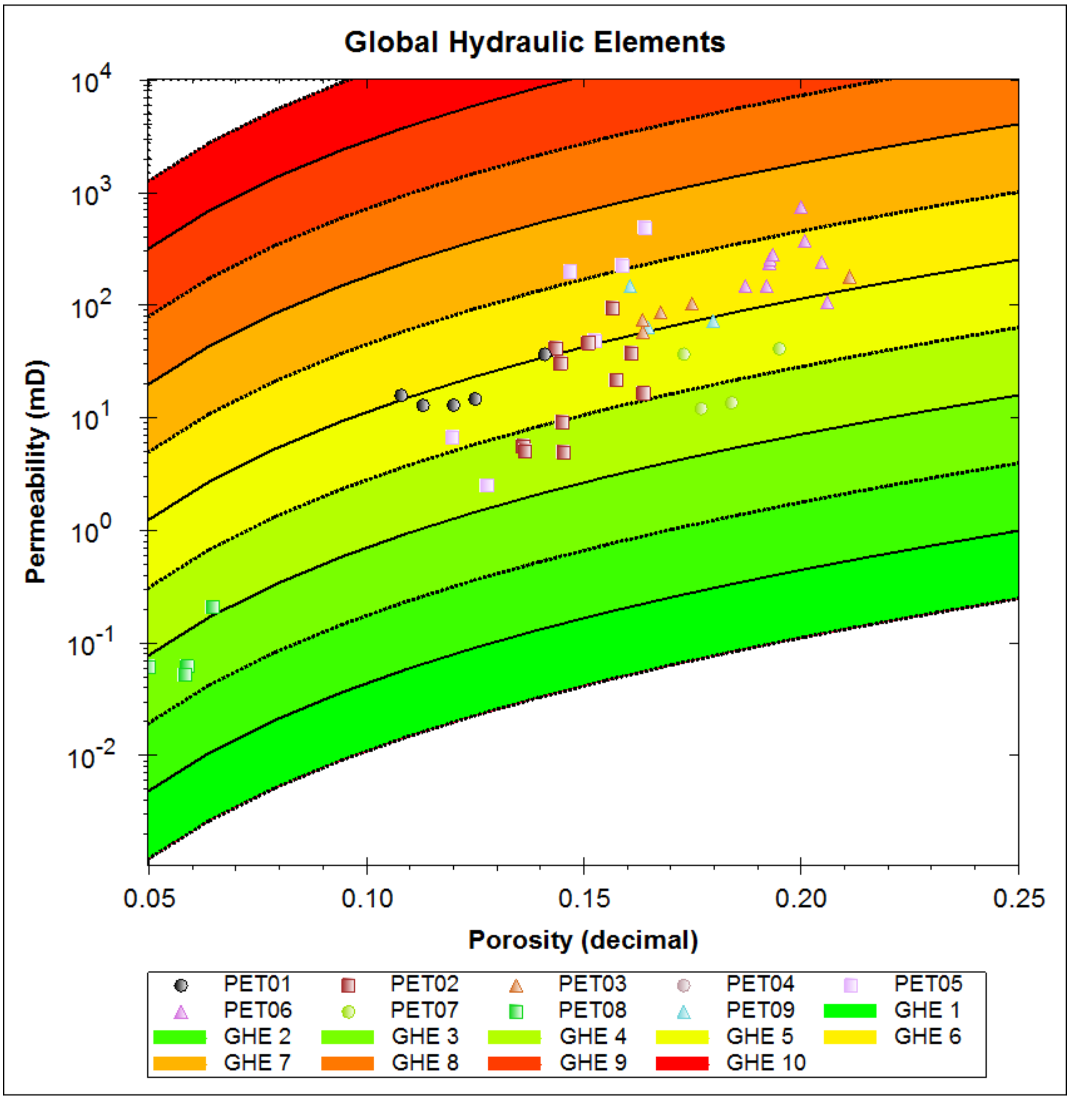

Figure 4–Plot of all the samples on a GHE graphic which serves as a basis for identifying individual of porosity-permeability clusters and closely related (in petrophysical space) samples in a systematic way, helping the recognition of petrophysical facies.

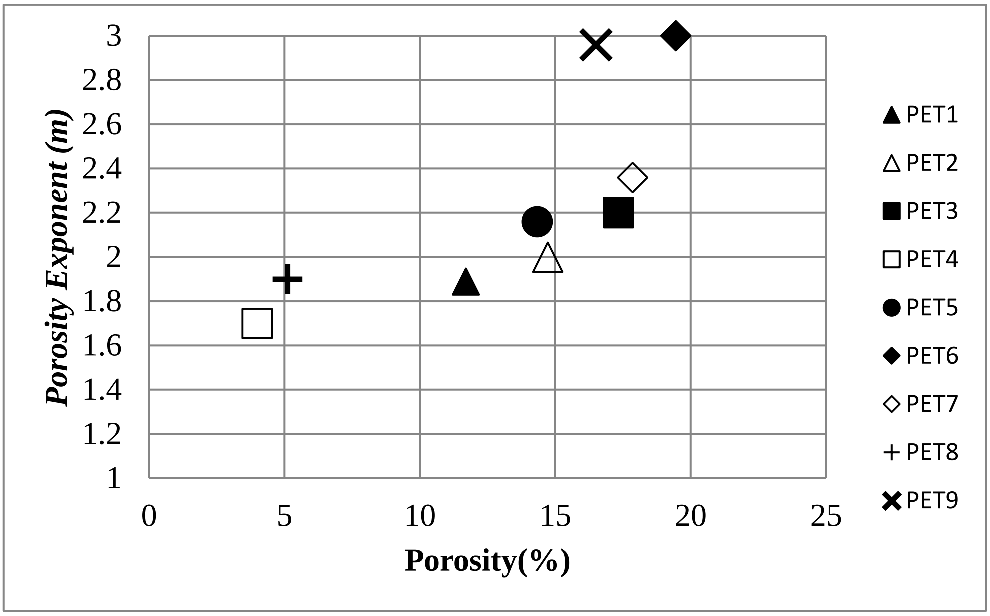

Figure 5 – Core Plug Measurements of Porosity Exponent vs Porosity – Morro do Chaves Formation.

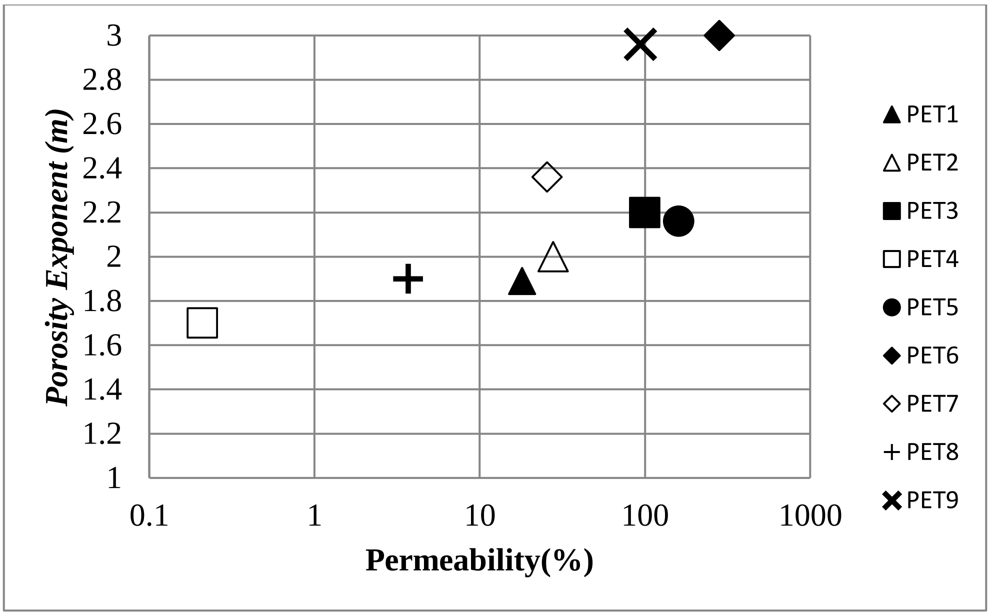

Figure 6 –Core Plug Measurements of Porosity Exponent vs Permeability – Morro do Chaves Formation.

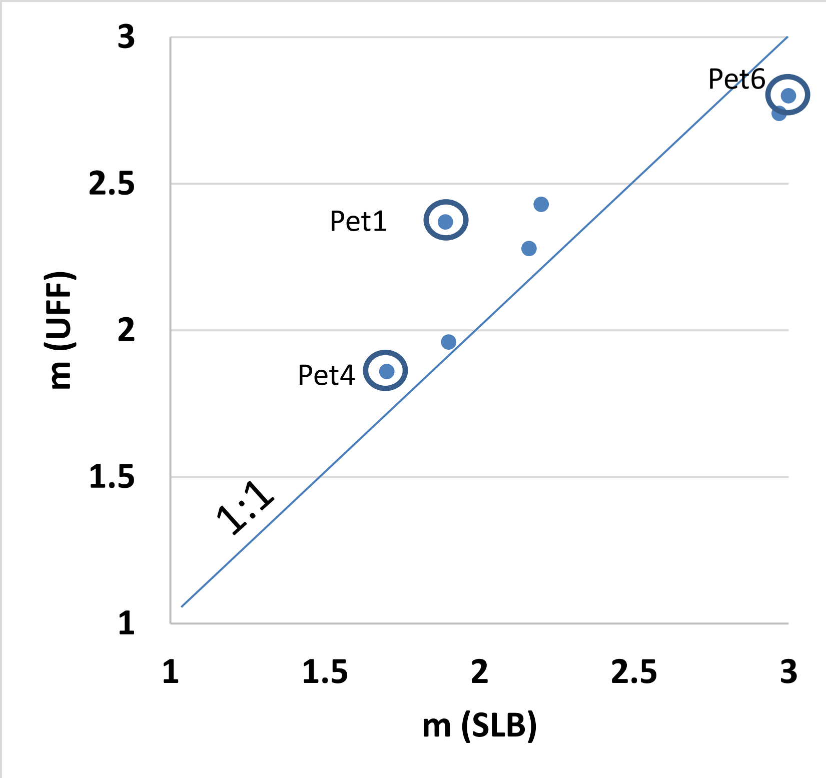

Figure 7 - The measured porosity exponent (*m*) values for Coquina samples (samples PET 1, PET 4 and PET 6 from Câmara et al., 2014, Wang et al., 2015). Measurements in the UFF (*m* UFF) and the Schlumberger laboratories *(m* SLB) are comparable. Included are some other coquina PET samples not studied in further detail. The 1:1 line is shown for reference.

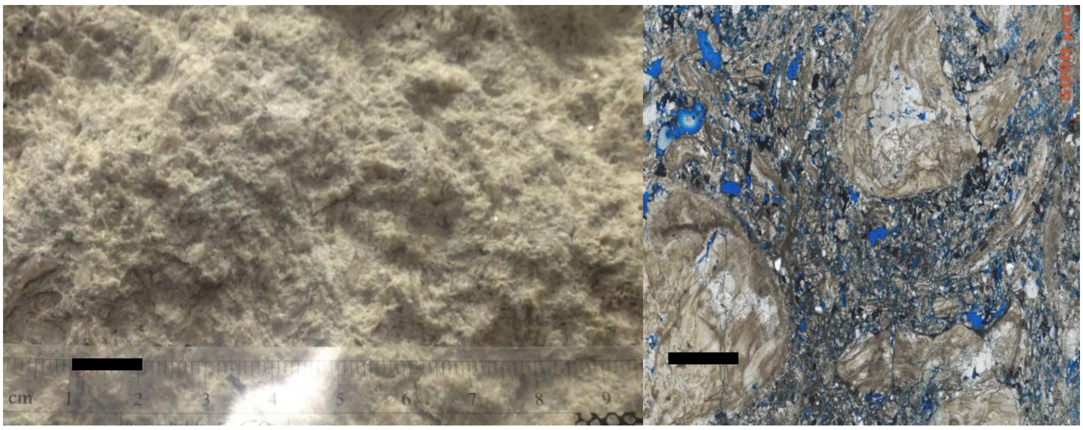

Figure 8 – PET 1. Calcirudite of whitish cream to light grey colour, bioclastic, fine to very coarse, poorly sorted, normally compacted, predominantly point and longitudinal contacts. The photo on the left shows a representative hand sample of the facies (scale bar 1cm), the photo on the right is a typical thin section of PET1 (scale bar 0.2cm) with porosity shown in blue.

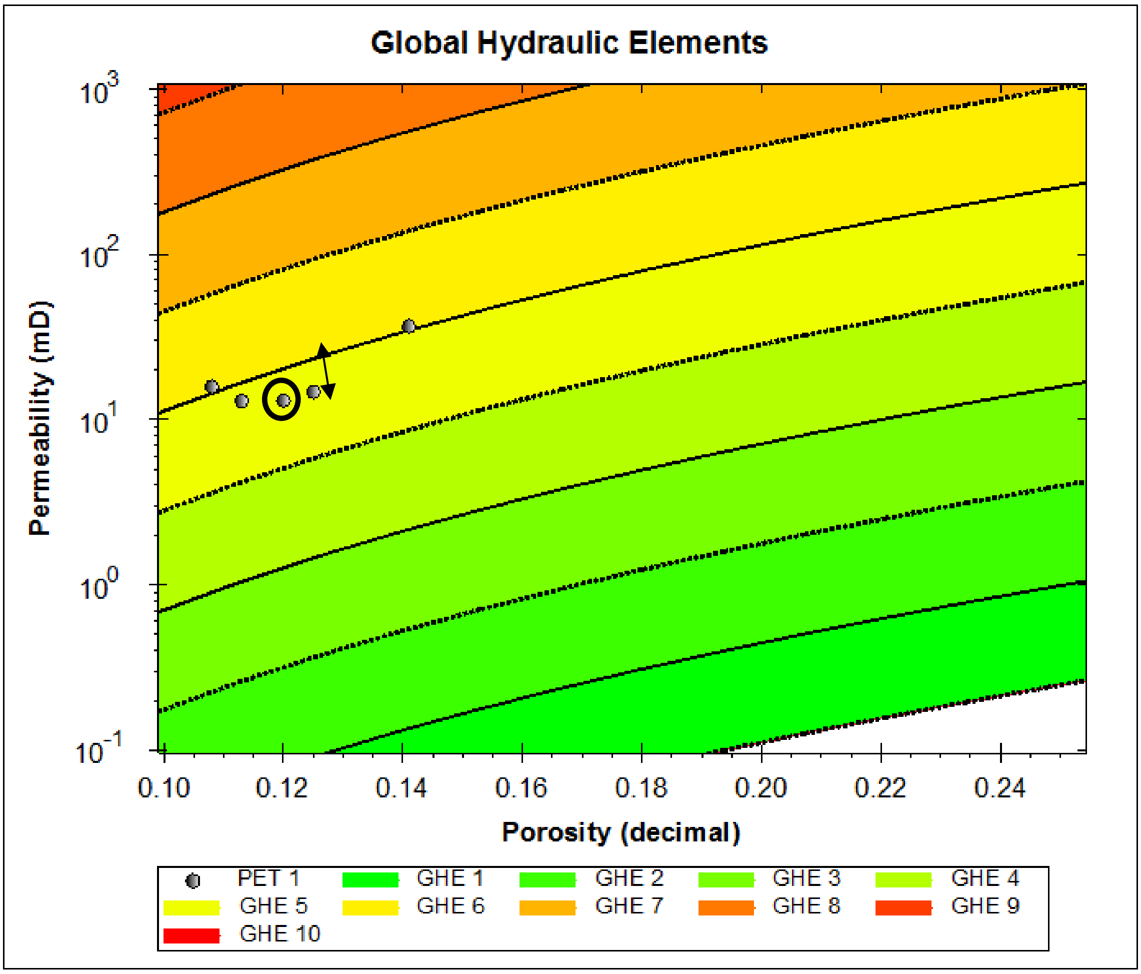

Figure 9 – PET 1. GHE plot showing reasonable porosity and permeability largely within GHE 5. The arrow highlights the relatively narrow spread of data for this petrotype. Selected PET 1 plug sample for this study circled.

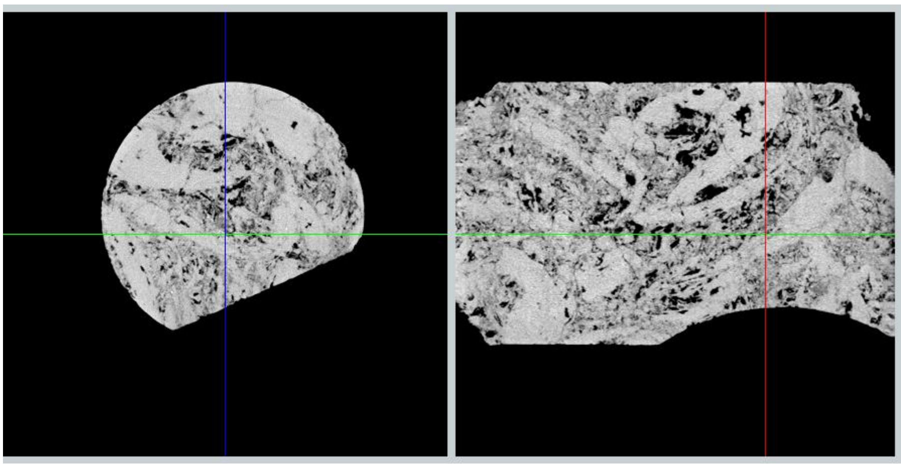

Figure 10 – PET 1. Micro-CT image of PET-1. (NB: 1inch diameter core plug) This CT image is from an offcut of the measured plug – which was a regular cylinder.

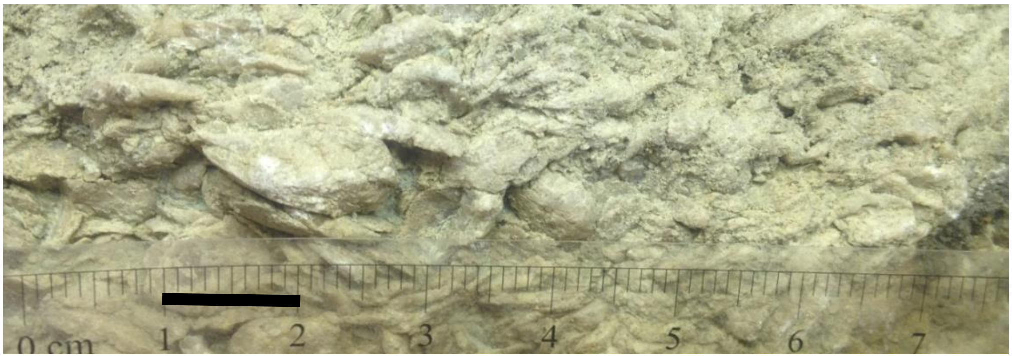

Figure 11 – PET 4. Calcirudite of whitish cream to light grey colour, bioclastic, fine to very coarse, poorly sorted, sub-rounded to angular, densely compacted (Fitted fabric), predominantly concavo-convex contacts. Scale bar 1cm.

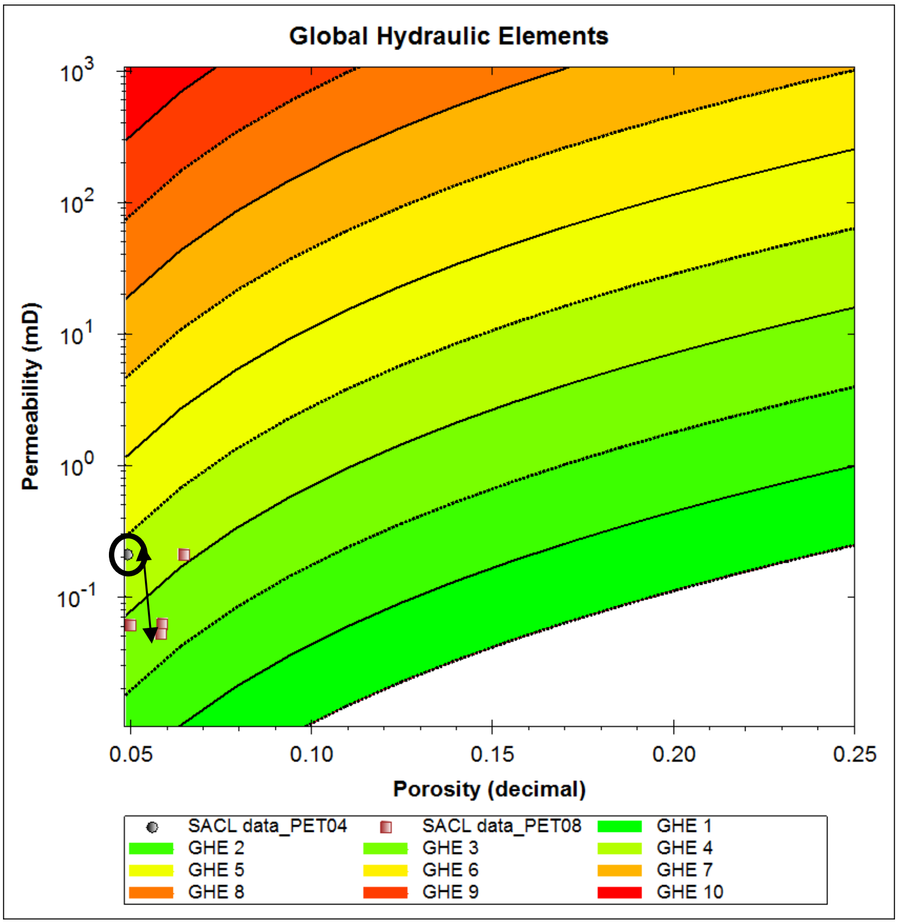

Figure 12 – PET 4. GHE plot showing the characteristic low porosity and permeability of PET 4 and sample PET 8. Selected PET 4 plug sample for this study circled.

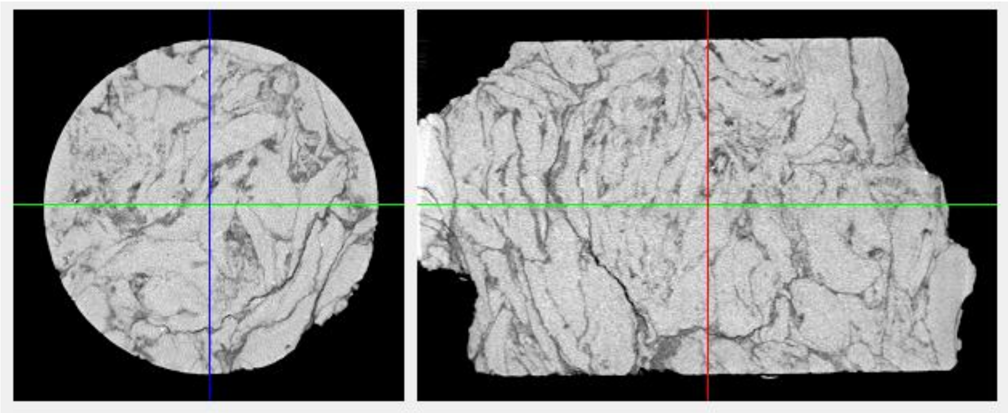

Figure 13 – PET 4. Micro-CT image of PET 4 – showing a fitted fabric and the presence of fractures/stylolites/dissolution seams. Micro-CT estimated porosity: 3.85%; Porosity from Porosimeter: 4% - suggesting a possible 0.15% porosity under 40μm (the resolution of the micro-CT). (NB: 1inch diameter core plug). Note this CT image is from an adjacent untrimmed twin plug close to the measured plug and shows dissolution seam related 'fracturing'.

Figure 14 – PET 6. Calcirudite, light cream to white, bioclastic, with fine pebble size, moderately sorted, sub-rounded, loosely compacted, predominantly point and longitudinal contacts (scale bar 1cm).

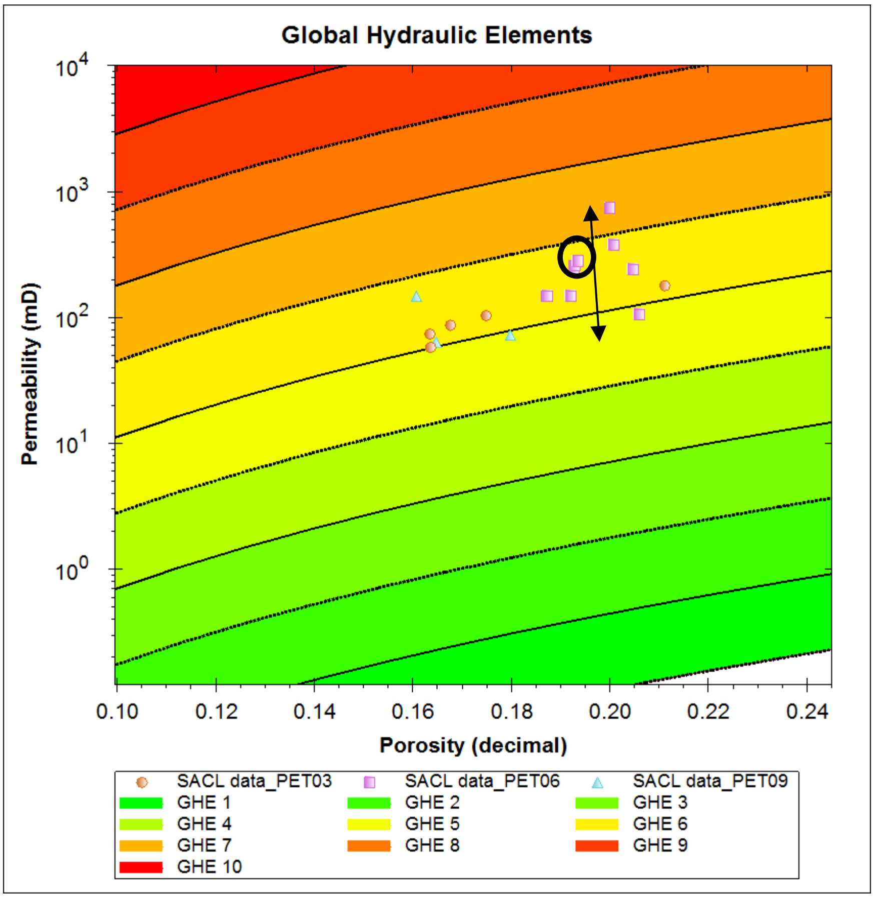

Figure 15 – PET 6. GHE Plot showing good porosity and permeability dominantly within GHE 6. The arrows shows the spread in this one sample as a result of the moldic nature of the pore types. Selected PET 6 plug sample for this study circled.

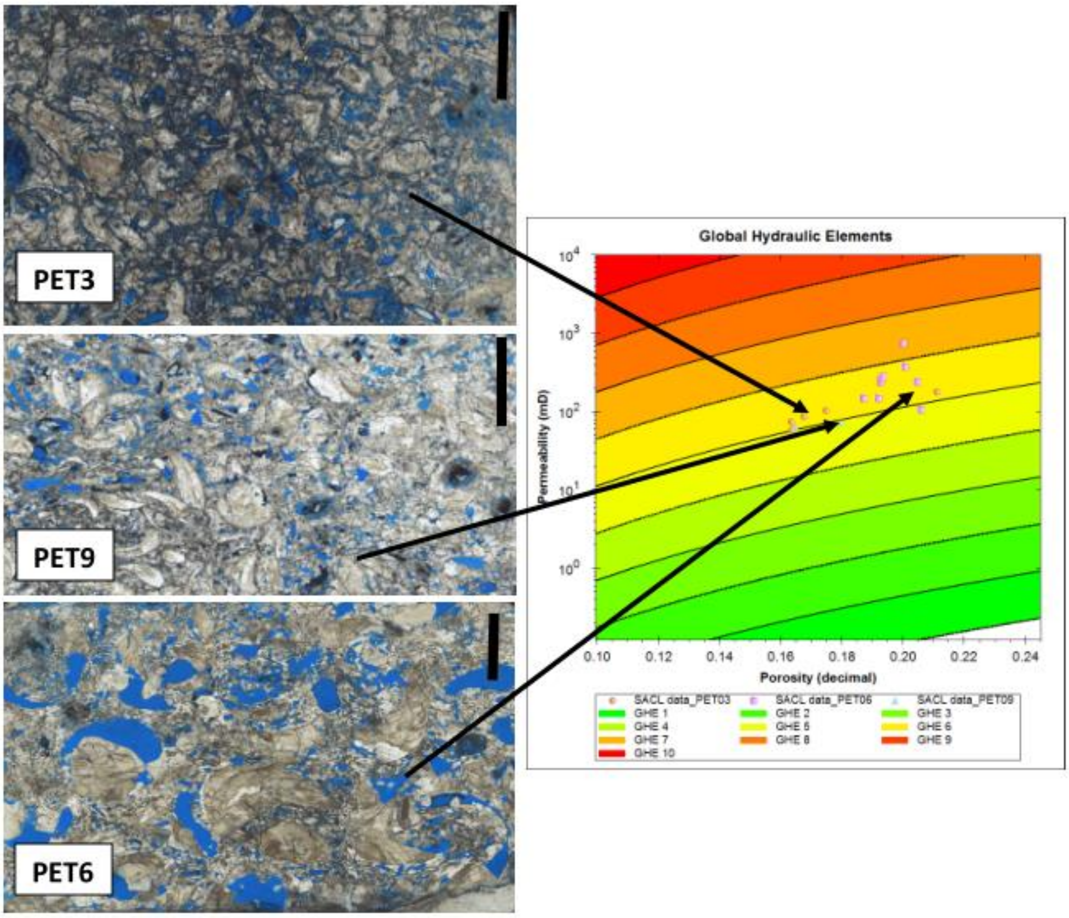

Figure 16 – Petrographic thin sections representative of PET 6 (in relationship to PET 3 and 9) showing the relationship of porosity with depositional energy, as the larger the shell size the larger the subsequent moldic porosity. On the right side, the GHE plot shows the relationship of porosity and permeability, and it can be observed that permeability range is limited to one order of magnitude whilst the porosity is varying from 16.51 to 21.1%, and this variation in porosity is controlled by the shells (bivalves). Blue is porosity. Scale bar 0.5cm.

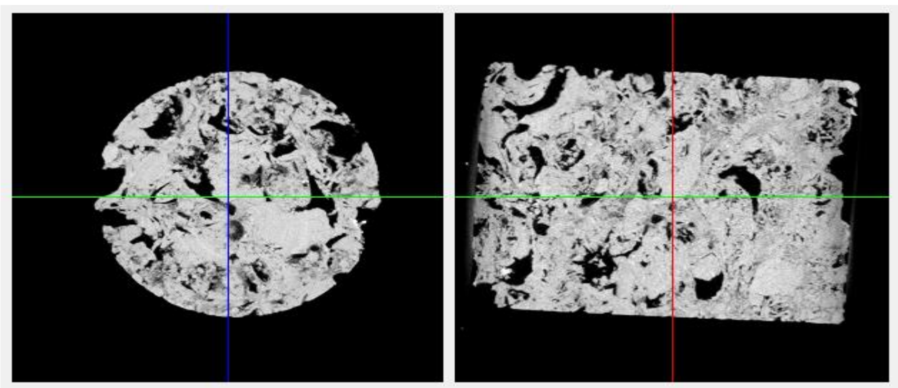

Figure 17 – PET6. Micro-CT image of PET6 – showing large dissolution pores. (NB: 1inch diameter core plug). It is more apparent than in the thin sections that some of these pores might be isolated or partially isolated. Note these CT volumes are from offcuts of the measured plugs.

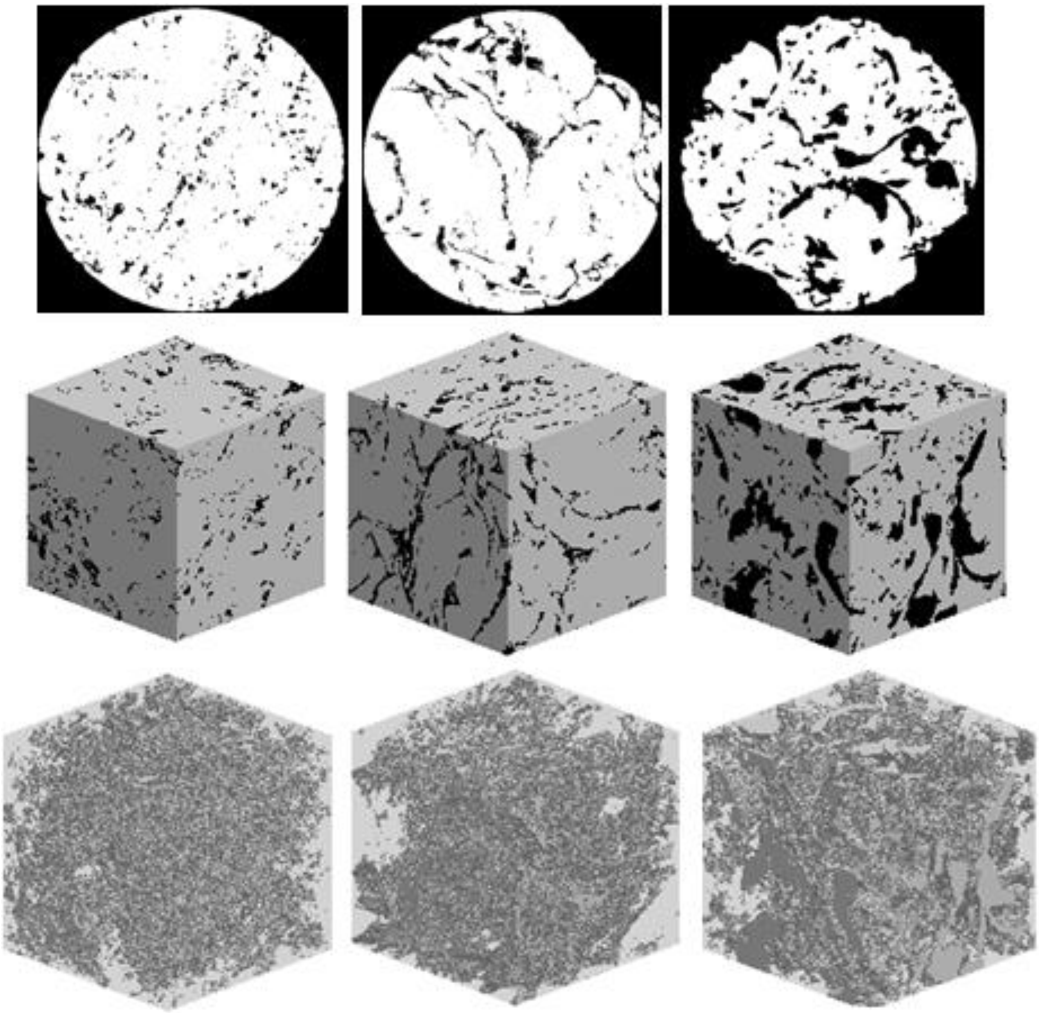

Figure 18 - The micro-CT cross sections for Coquina samples (PET 1, PET 4 and PET 6 from Câmara *et al.*, 2014; Wang *et al.*, 2015). Their resolution are 19.04 μm, 20.44 μm and 19.27μm from left to right. The sizes of the CT images for these three samples are 2240x2240x1411, 1440x1440x1261 and 1968x1968x1975 voxels respectively. Each plug is either 1in diameter, offcuts from the plugs used for the Formation Factor experiments. The segmentation results of PET1, PET4 and PET6 are shown in cross section (top), 3D cube (middle) and pore space visualization (bottom). The 3D cubes (800x800x800voxels) for these three samples are chosen from their CT images. (Wang *et al.*, 2015)

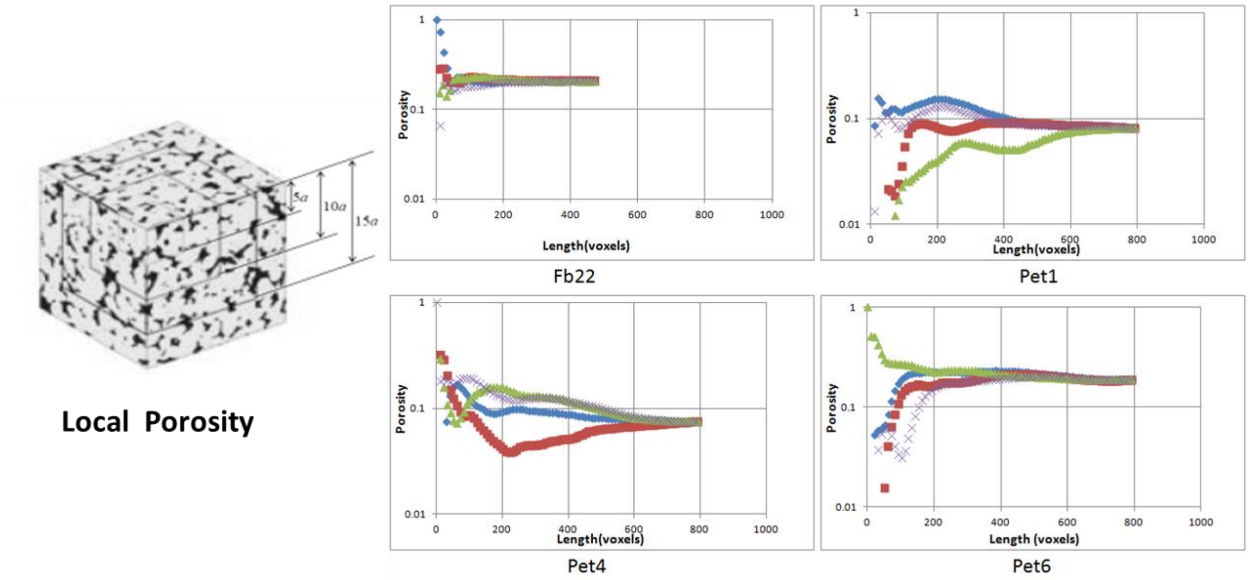

Figure 19 – Definition of sample volumes (left) and variation in porosity estimates with varying scale (right). The sandstone has an REV less than 200voxels. For these coquinas it is occasionally from 250 voxels but generally more than 600voxels.

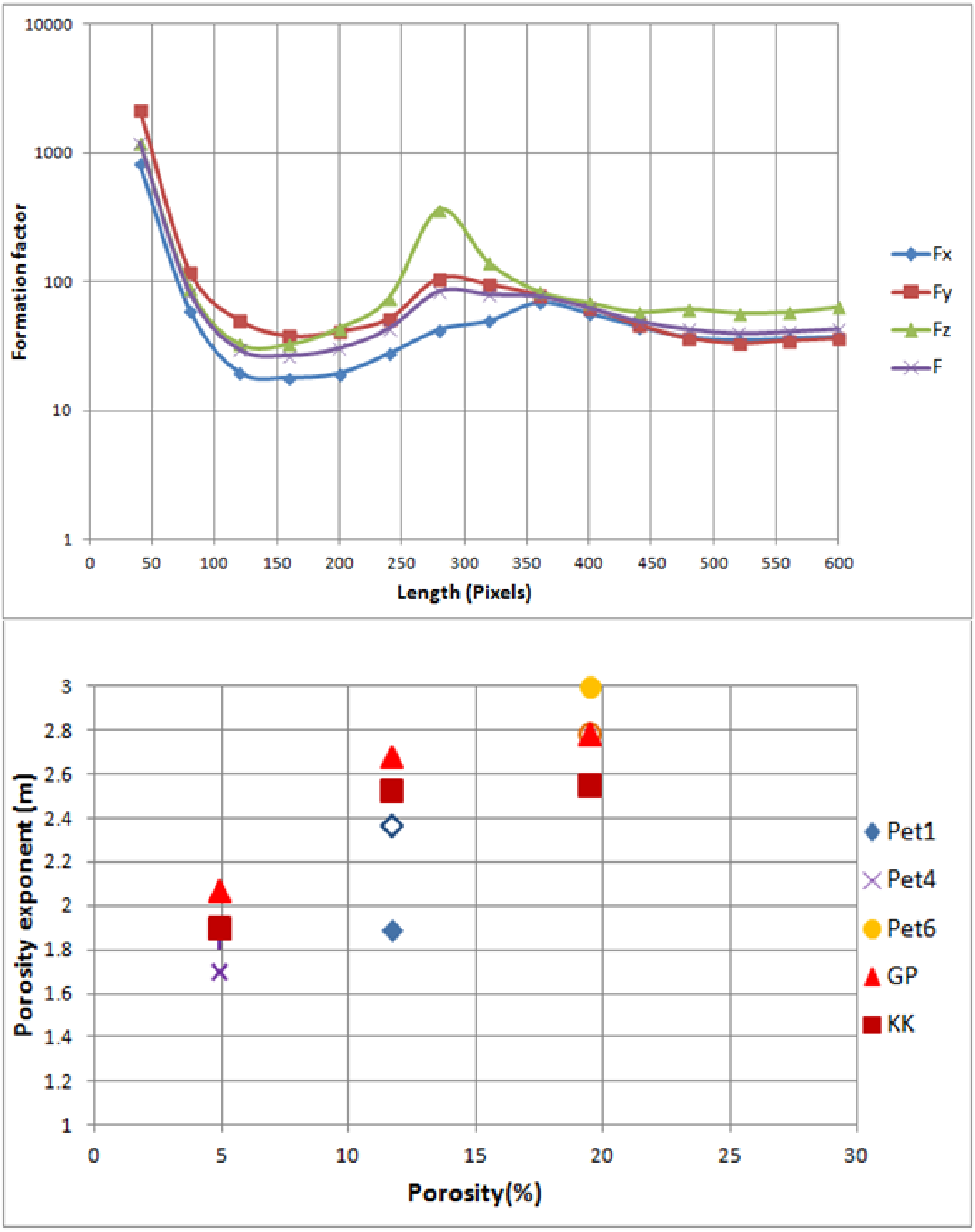

Figure 20 – Measurements (identified as PET 1, PET 4 and PET 6) compared with numerical simulation results (GP, KK) of the porosity exponent in coquina samples. Top: To evaluate the REV the formation factors of 15 sub samples were calculated in three directions and the formation factors versus the length of the samples united by the pixel number is in top picture. When the number reaches ca. 350, the formation factors are gradually convergent. Bottom: The results of the numerical models compared with data. The estimation of porosity exponents based on a renormalisation method with two calculation algorithms denoted by GP and KK. In the bottom picture, the estimation results from average of eight sub samples with REV selected at 600x600x600voxels. (Wang 2015 and Wang *et al.*, 2015). There are two values for *m* measured from the different labs and the simulations consistently get better matches in PET 4 and 6.

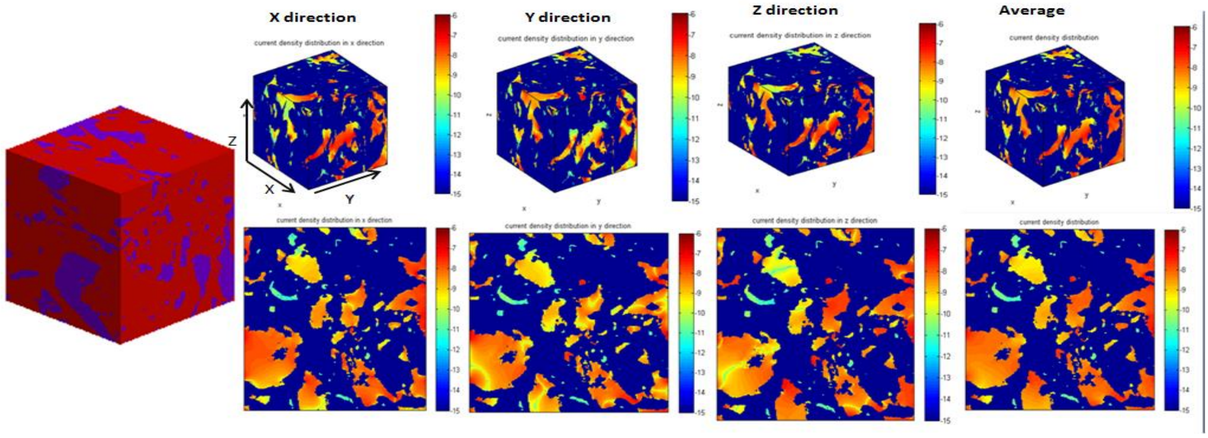

Figure 21 - The current flow density distribution from a sub sample of PET 6. The binary image consists of pore in blue and matrix in red. In the current density distribution, the legend is based on logarithm10 scale, the direction of the current flow is in x, y, and z from left to right respectively and the pictures of the final column are the average results for 3D and 2D. Pale cool colours show isolated pores.

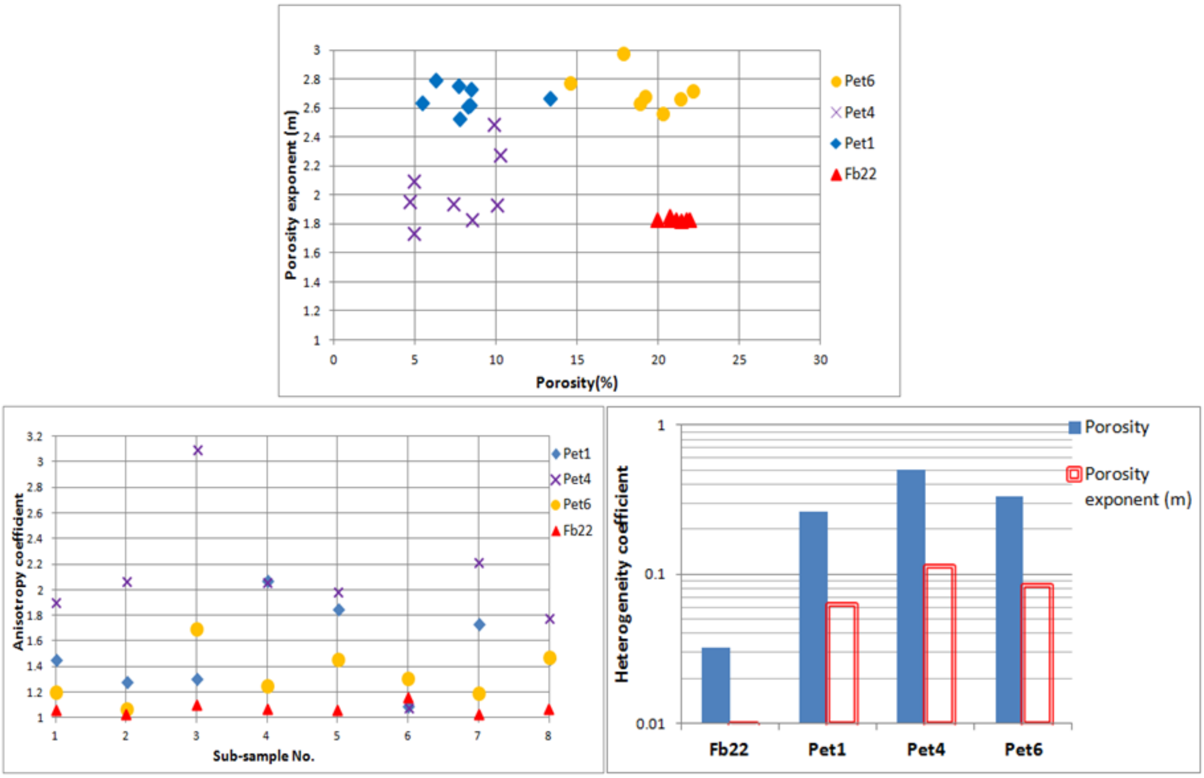

Figure 22: Heterogeneity and anisotropy of porosity exponent, *m*. Top: The distribution of the average porosity exponents for a sandstone (sample Fb22) and coquina carbonates PET 1, PET 4 and PET 6. Bottom left: The anisotropy coefficient based on the porosity exponent in three directions for the eight REV samples and Bottom right: heterogeneity coefficient (standard deviation /average) for both porosity and porosity exponent for these eight REV samples (Wang 2015 and Wang *et al.*, 2015).

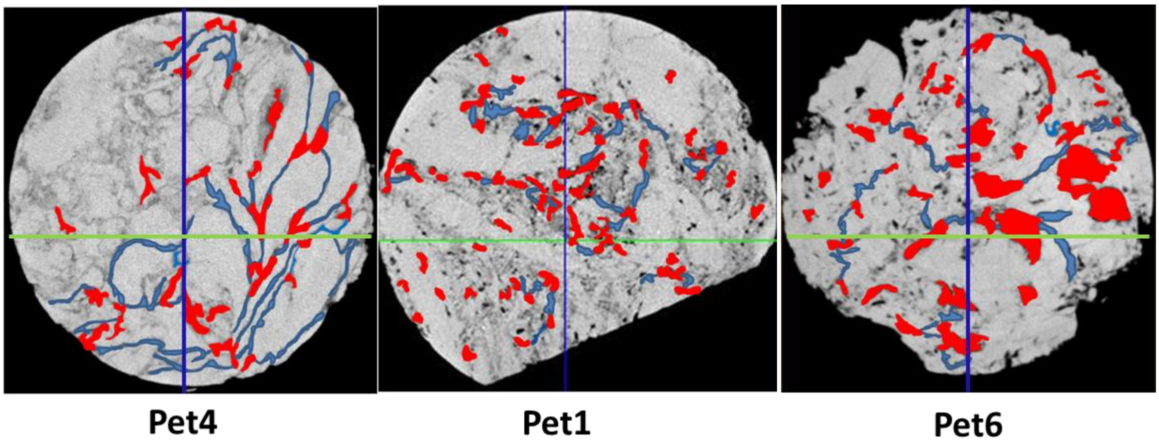

Figure 23 – Illumination of pores (in red) and pore throats (blue) in three coquina samples from the Morro de Chaves Formation (From Wang, 2015). Fracture-like pore throats (in blue/light grey) connecting the pores are seen in Pet4 (relatively low *m*) and the large angular, moldic, complex pores (in red/dark grey) are seen in PET6 (relatively high *m*). The IG pore/throat system of PET 1 is distinctly different and represents a more normal "Archie" rock with *m* closer to 2.

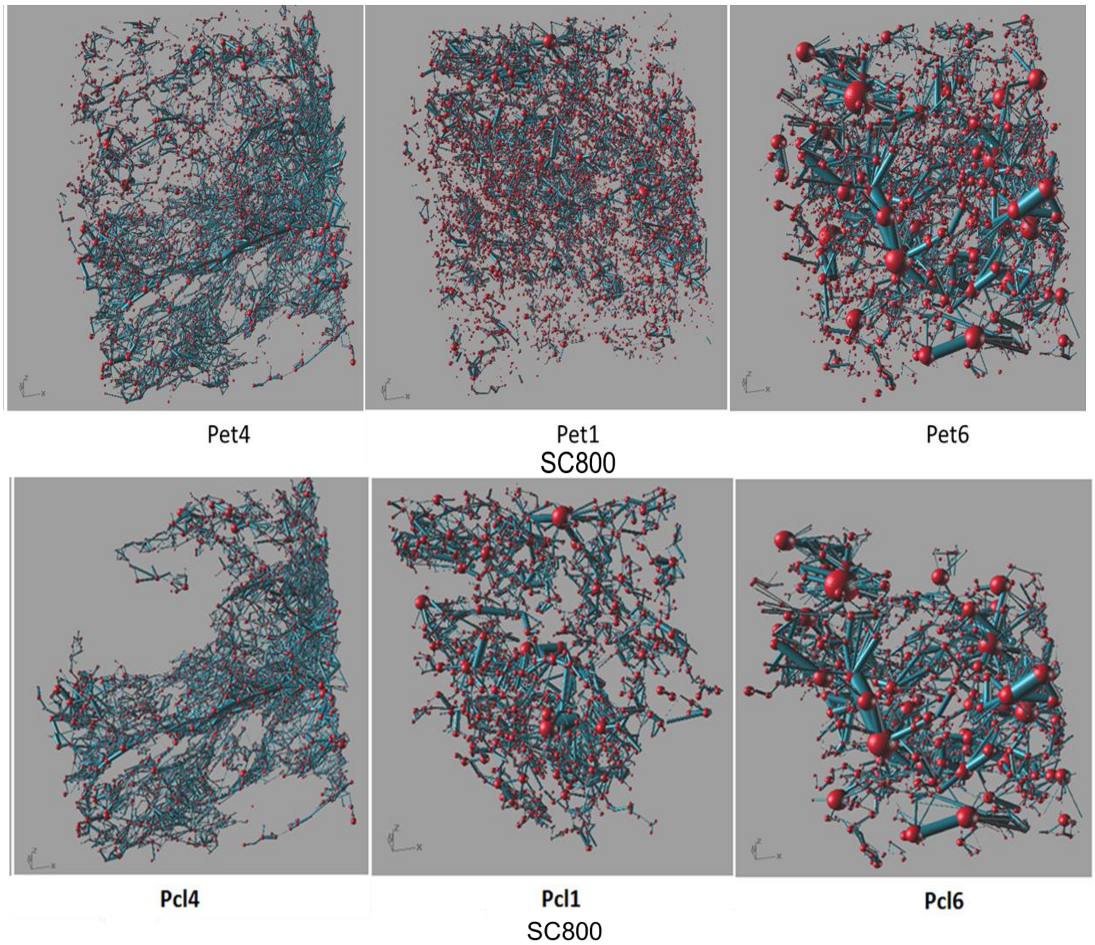

Figure 24 – Pore (red) and pore throat (blue) representation of the (above) complete network and (below) the spanning cluster for the 3 samples (PET 4, PET 1 and PET 6) (see Wang 2015). PET 4 has a discrete concavo-convex pore network. Network size extracted from micro-CT is 800x800x800 voxels.

TYPE OF POROSITY	PICTURE	*m*
Moldic Unconnected **(>10% OF UNCONNECTED POROSITY)**	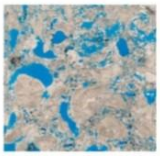	**2.2-3.0**
Moldic Connected **(<10% OF POROSITY UNCONNECTED)**	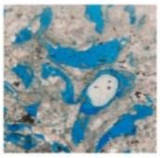	**1.8-2.2**
Intergranular	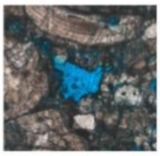	**1.95-2.05**
Intercrystalline	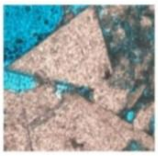	**1.9-2.10**
Fracture		**1.7-1.9**

Figure 25 – Summary of porosity exponents (*m*) and the dominant pore type in the coquinas of the Morro do Chaves Formation (Câmara, 2013). The 'fracture' category here is actually a relatively planar discontinuity sometimes related to solution seams.

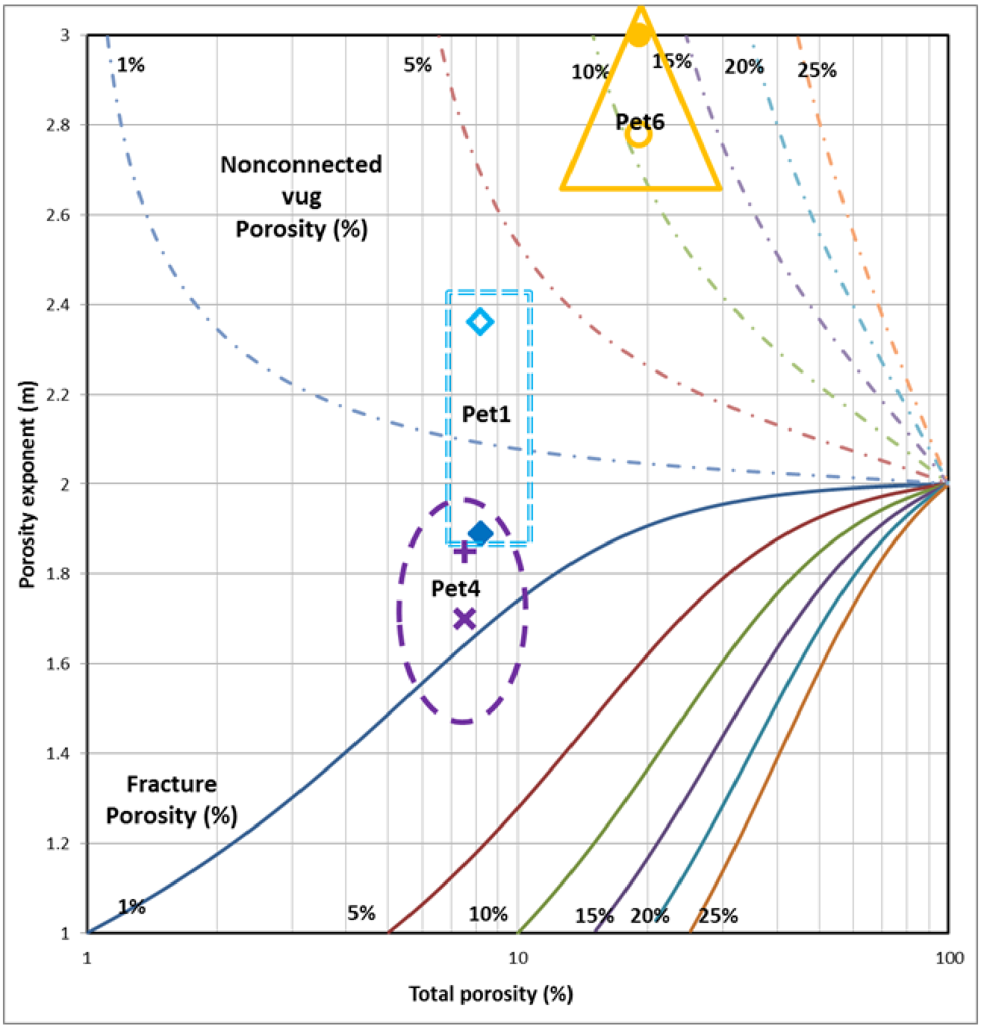

Figure 26 Aguilera and Aguilera (2003) model for double matrix systems containing fractures or non-connected vugs (in their published terminology, but in this study large pores are predominantly moldic) showing the position of the three coquina samples in this study. In each case the two values for *m* represent maximum and minimum observed values.

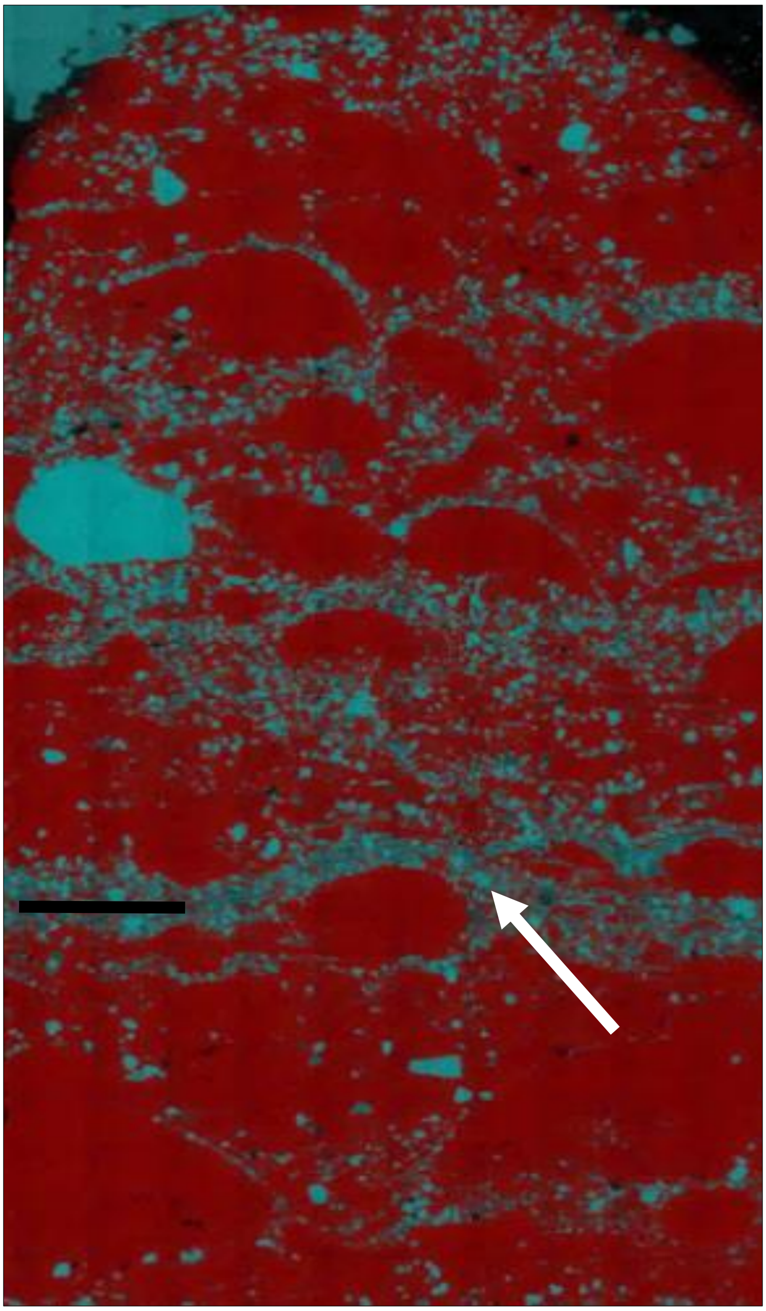

Figure 27 Energy-dispersive X-Ray (EDX) image for a sample (PET8) from the Morro do Chaves. Red (dark) material is calcite, and the blue (lighter) quartz, showing concentrations of quartz along dissolution seams (image courtesy of Jim Buckman) where inter-granular porosity is developed. This sample is very similar in characteristics to PET 4 (Fig. 12). White arrow indicates a major solution seam, scale bar is 0.2cm. From Mitchell, 2014.

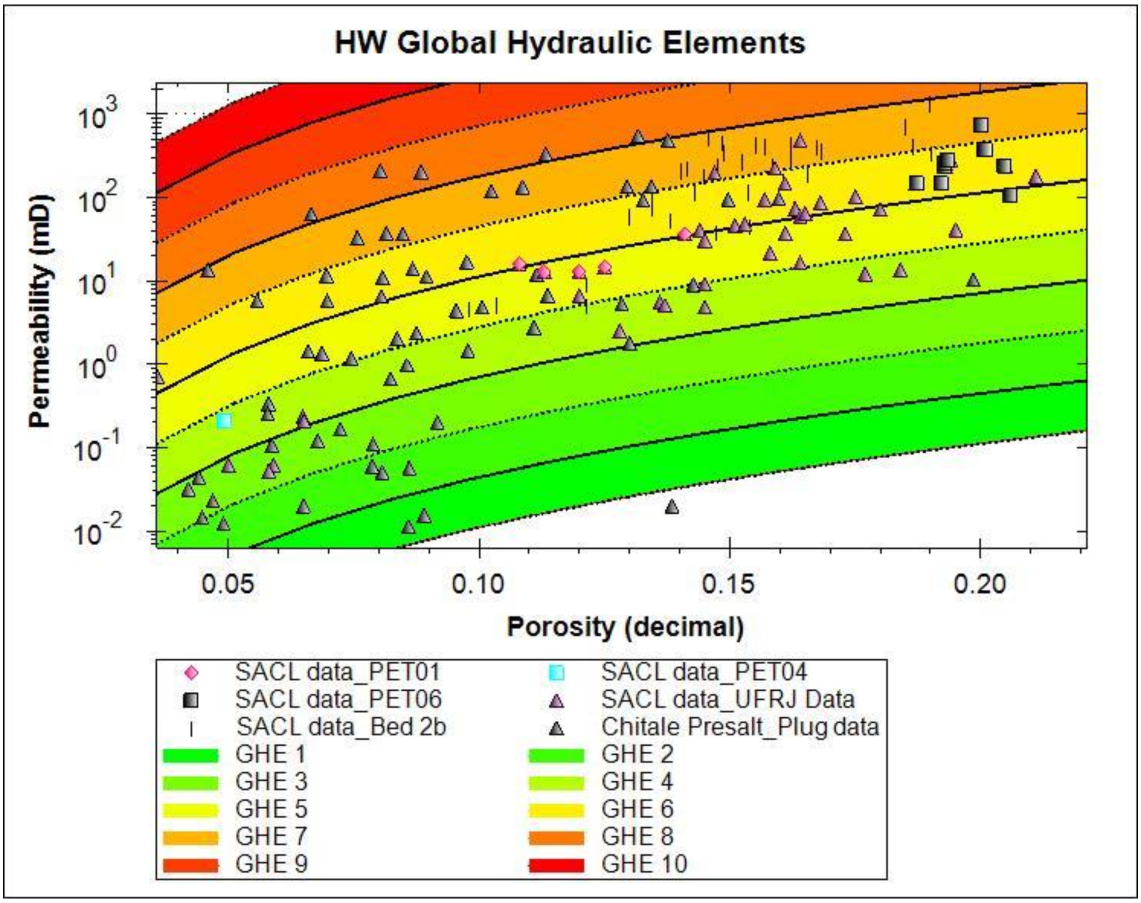

Figure 28: Summary plot of core data from the Sergipe-Alagoas Carbonate Laboratory including PET 1, 4, 6 and previously published Bed 2b (Corbett et al., 2016) together with published pre-Salt data from the Campos Basin (Chitale *et al.,* 2015) allowing the reader to see the representivity of the plugs detailed in this study. Note; that the Chitale rocks are not coquinas but represent one of the few published poroperm data sets from the pre-Salt in Brazil and well illustrate the variability these reservoirs encounter.

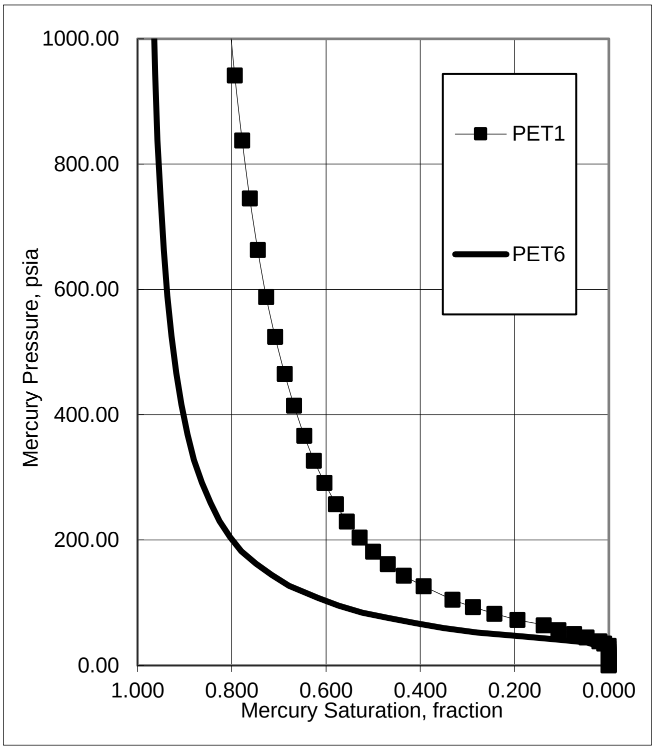

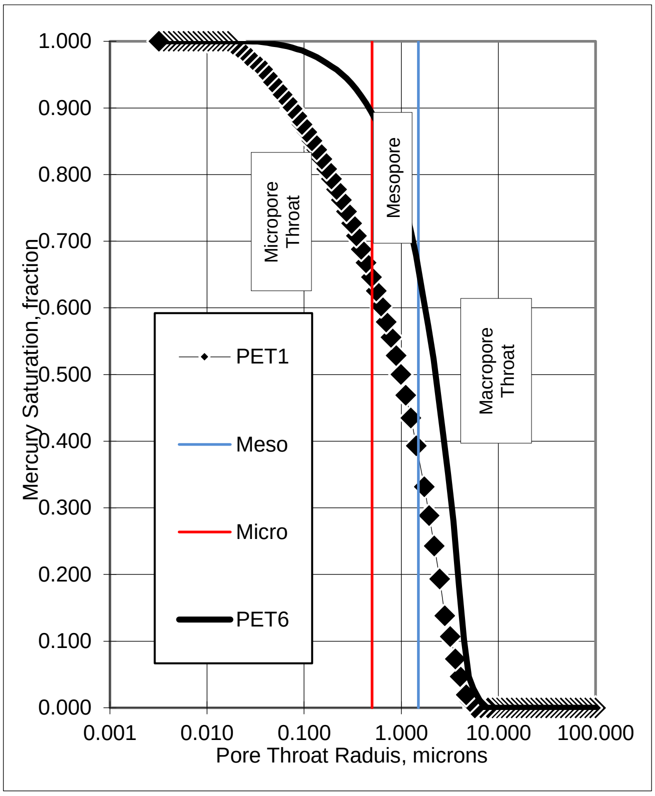

Figure 29: Mercury Injection data for PET 1 and PET 6. No data were available for PET 4 because of budgetary limitations for this study. Note the smaller contribution of micro-porosity in PET 1 relative to PET 6 as shown in the lower plot.

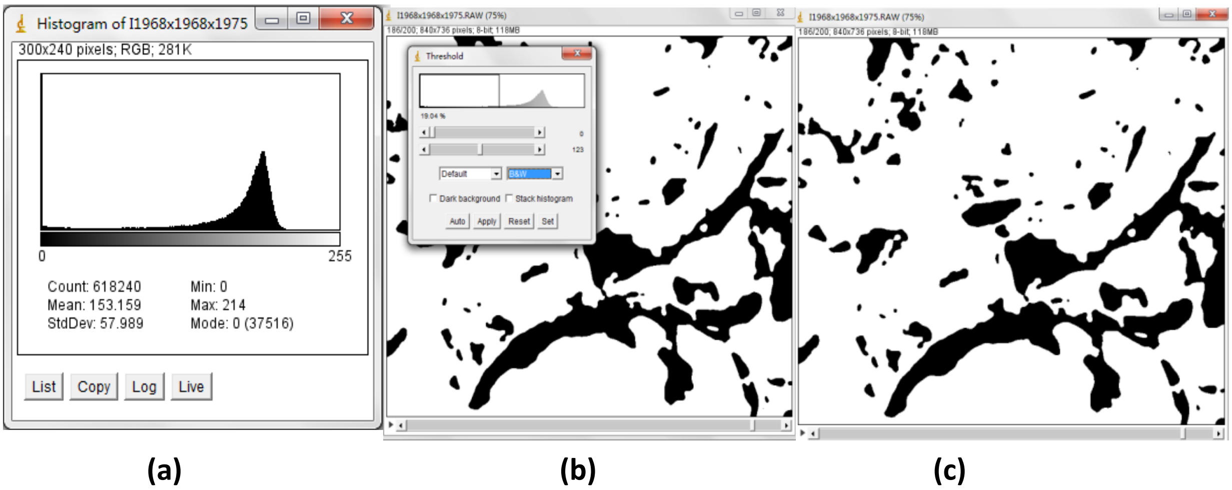

Figure A1: The histogram of the images which can be used to offer threshold. If the threshold is difficult to extract from the histogram, the threshold can be chosen by comparing the difference of segmentation results with variable thresholds using the “Threshold” dialogue in (a) and (b). Image (c) is the binary image from auto threshold using the ”Auto” function for comparison.

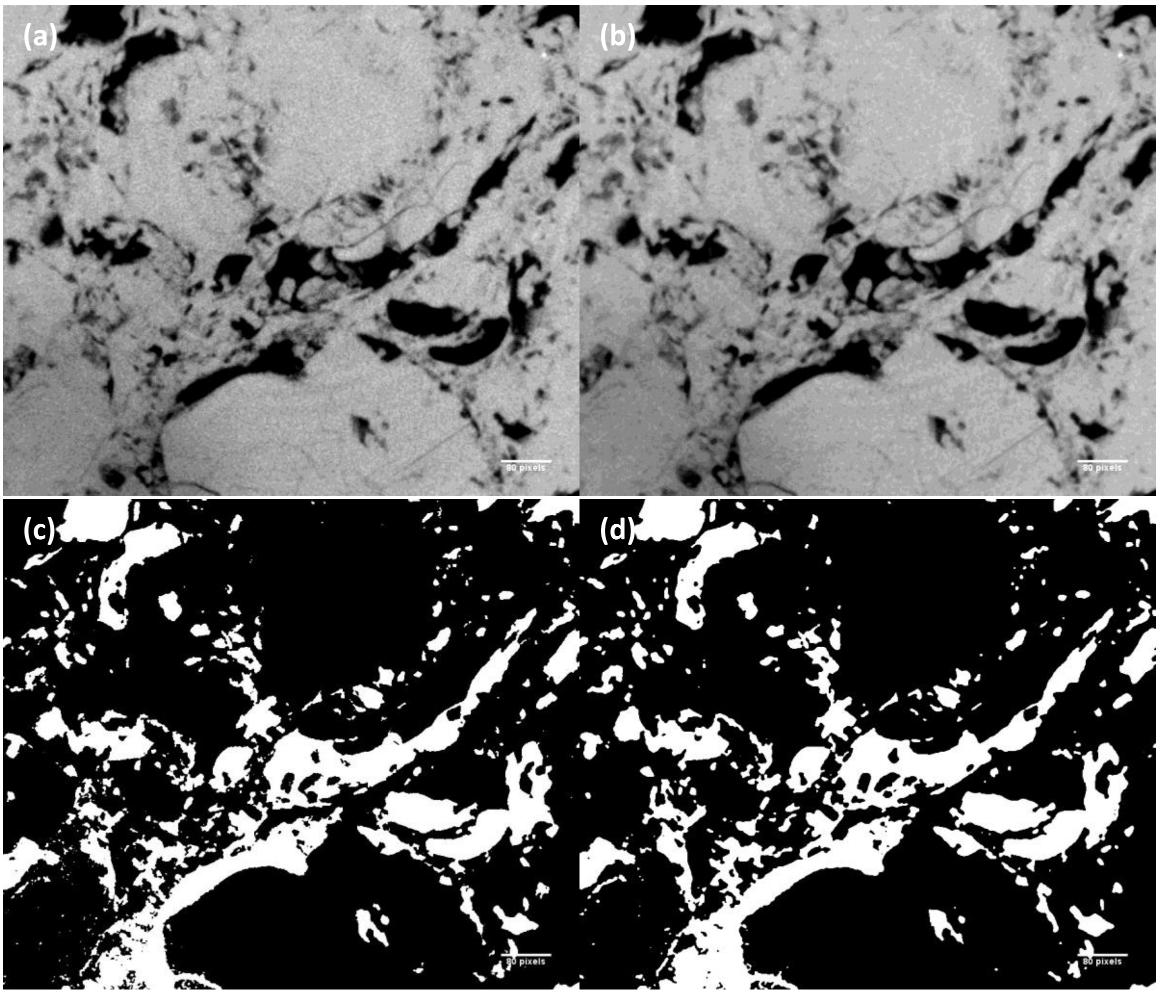

Figure A2: Images showing the result of the of median filter shown by comparing (a) the original grey-scale CT image cross section with (b) the filtered CT images, and their related binary images in (c) and (d) respectively. This shows that little fidelity is lost by the employement of the filter.

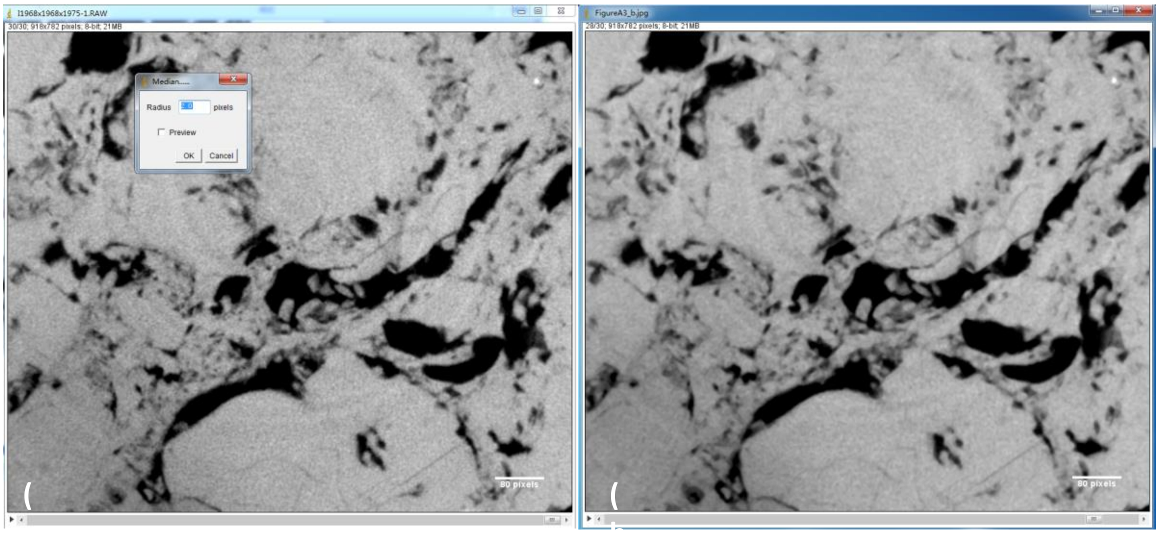

Figure A3: The cropped images can be filtered by the media filter by setting the radius of the filter. The effect of median filter can be shown in this figure. The noise in (a) can be smoothed (b).

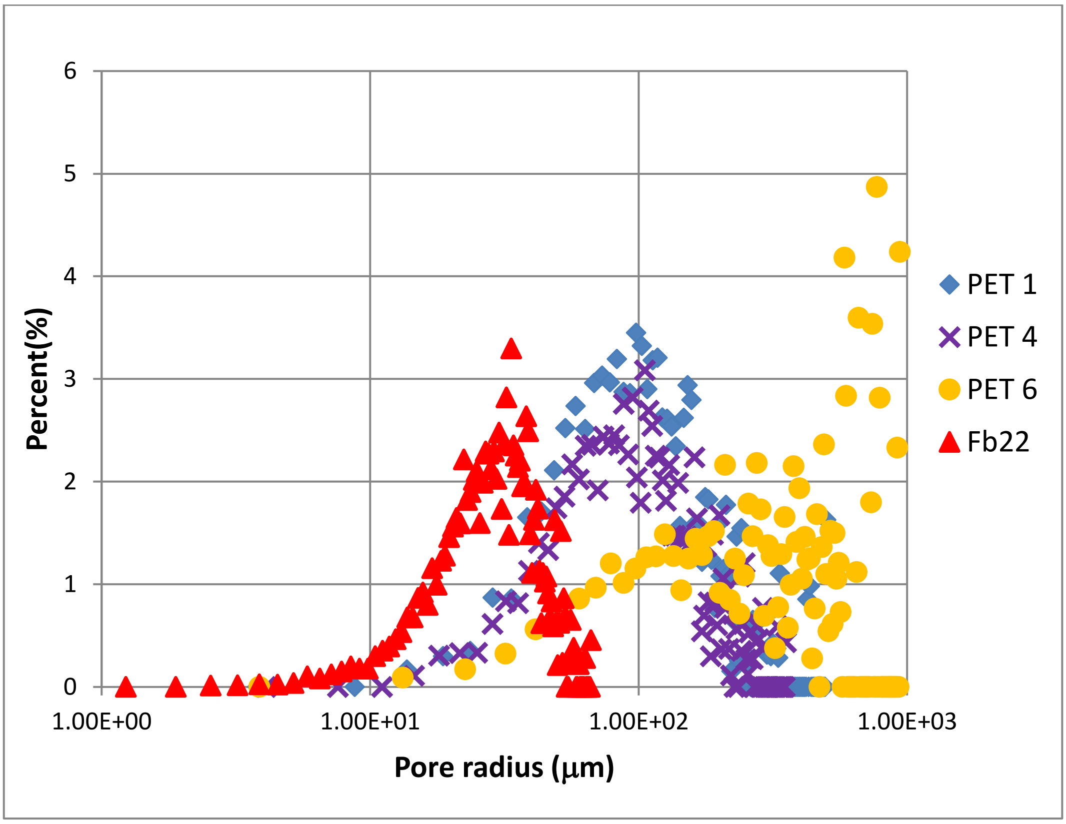

Figure A4: The pore size distribution for PET1, 4 and 6 (400 voxel cube size) and Fb22 (240 voxel cube). The x-axis is shown in logarithm and y-axis is the percentage (%) of each radius. Note that Fb22 has a much smaller distribution.

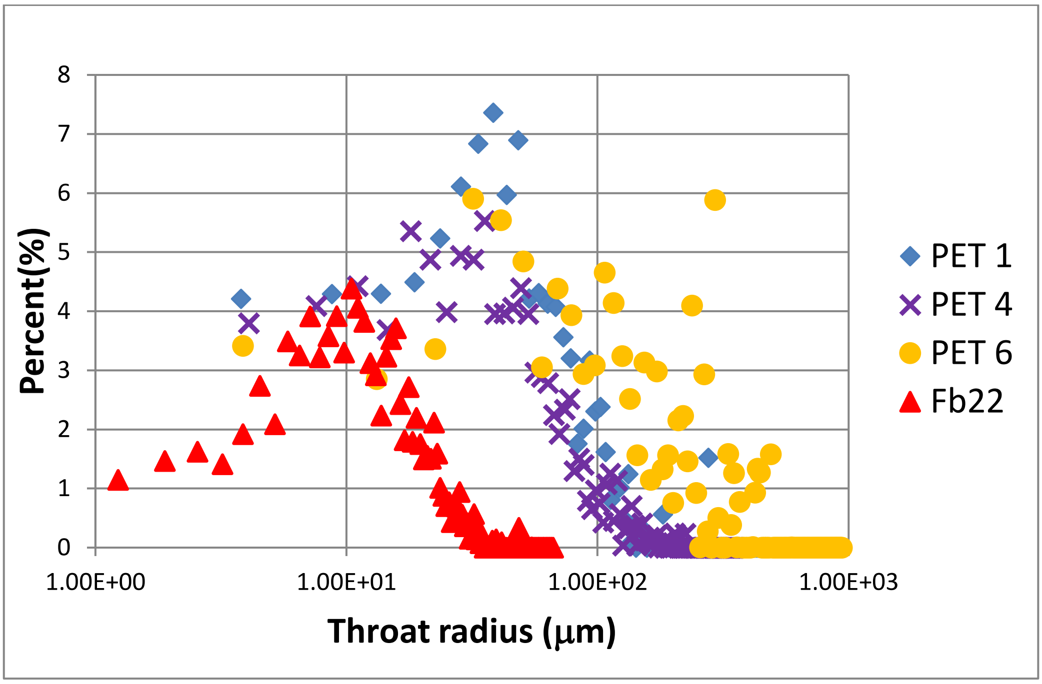

Figure A5: The throat size distribution for PET1, 4 and 6 and Fb22 (refer to Fig. A4).

.

Sample	micro-CT (%)	Porosímeter (%)
PET 1	9	12
PET 4	7	5
PET 6	15	19,5

Figure A6: Comparison of micro-CT and porosimeter porosity for adjacent offcuts (micro-CT volumes) from core plugs (the adjacent plug volumes). Given the variability in carbonates these results suggest that the micro-CT is not ‘missing’ significant porosity, particularly in PET 4 which has the smallest pores and throats in these carbonates. (From Câmara, 2013)

Highlights

- Coquina carbonate pore types and petrotypes
- Use of resistivity measurements for geological 3D carbonate pore characterization
- Discussion of (non-)touching, (non-)connecting molds and vugs and petrophysical issues
- Carbonate reservoir characterization of solution seams

Graphical Abstract